*Nucleic Acids Research*, 2024, **52**, 11641–11658
https://doi.org/10.1093/nar/gkae731
Advance access publication date: 27 August 2024
**Genome integrity, repair and replication**

# Synergistic action of human RNaseH2 and the RNA helicase-nuclease DDX3X in processing R-loops

**Massimiliano Secchi†, Anna Garbelli†, Valentina Riva, Graziano Deidda, Carolina Santonicola, Teresa Maria Formica, Simone Sabbioneda, Emmanuele Crespan and Giovanni Maga***

Institute of Molecular Genetics IGM-CNR 'Luigi Luca Cavalli-Sforza', via Abbiategrasso 207, I-27100 Pavia, Italy

*To whom correspondence should be addressed. Tel: +39 0382546354; Email: giovanni.maga@cnr.it
†The first two authors should be regarded as Joint First Authors.
Present addresses:
Valentina Riva, Instituto de Medicina Molecular João Lobo Antunes, Faculdade de Medicina, Universidade de Lisboa, Lisboa 1649-028, Portugal.
Graziano Deidda, Diabetes Research Institute, IRCCS Ospedale San Raffaele, via Olgettina 60, I-20132 Milan, Italy.
Maria Formica, Division of Cardiology and Molecular Cardiology, Istituti Clinici Scientifici Maugeri, IRCCS, Via Maugeri 10/10A, 27100 Pavia, Italy.

## Abstract

R-loops are three-stranded RNA-DNA hybrid structures that play important regulatory roles, but excessive or deregulated R-loops formation can trigger DNA damage and genome instability. Digestion of R-loops is mainly relying on the action of two specialized ribonucleases: RNaseH1 and RNaseH2. RNaseH2 is the main enzyme carrying out the removal of misincorporated rNMPs during DNA replication or repair, through the Ribonucleotide Excision Repair (RER) pathway. We have recently shown that the human RNA helicase DDX3X possessed RNaseH2-like activity, being able to substitute RNaseH2 in reconstituted RER reactions. Here, using synthetic R-loop mimicking substrates, we could show that human DDX3X alone was able to both displace and degrade the ssRNA strand hybridized to DNA. Moreover, DDX3X was found to physically interact with human RNaseH2. Such interaction suppressed the nuclease and helicase activities of DDX3X, but stimulated severalfold the catalytic activity of the trimeric RNaseH2, but not of RNaseH1. Finally, silencing of DDX3X in human cells caused accumulation of RNA-DNA hybrids and phosphorylated RPA foci. These results support a role of DDX3X as a scaffolding protein and auxiliary factor for RNaseH2 during R-loop degradation.

## Graphical abstract

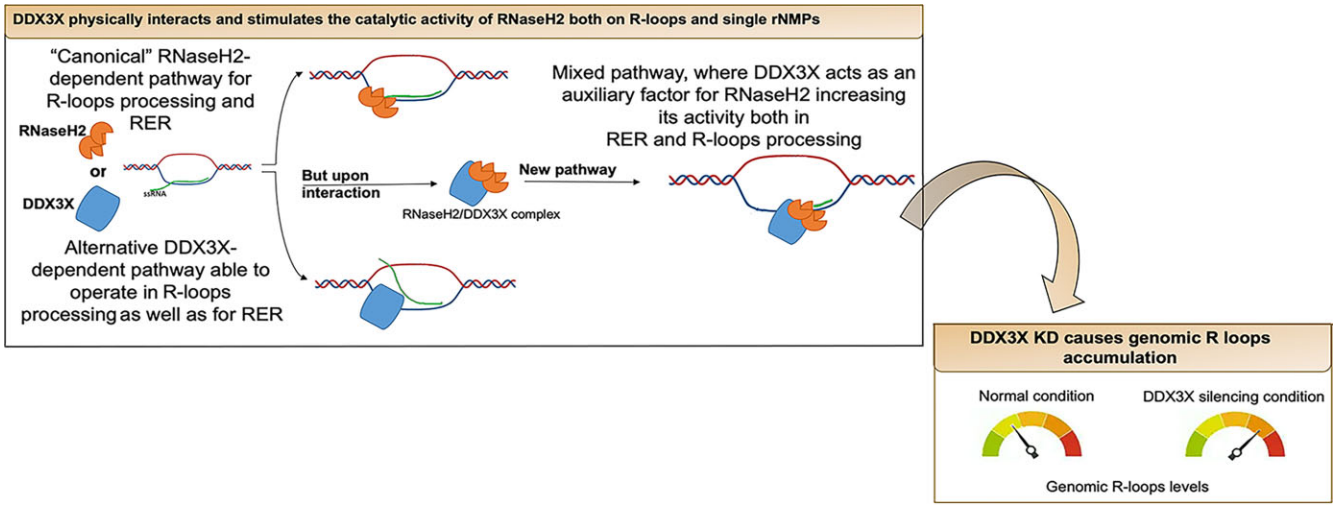


## Introduction

RNA–DNA hybrids formed through base pairing between RNA and DNA strands, are structures frequently found in eukaryotic cells under physiological conditions. Examples are the Okazaki fragments formed during lagging strand DNA replication or the RNA moiety of the telomerase complex annealing to the 3′-single stranded (ss) DNA overhangs of telomeres. A special class of RNA-DNA hybrids is the one where

**Received:** November 28, 2023. **Revised:** July 18, 2024. **Editorial Decision:** August 7, 2024. **Accepted:** August 12, 2024

the base pairing of the RNA strand occurs within a double stranded (ds) DNA region, causing the displacement of ssDNA. Such three-stranded structures consisting of an RNA–DNA hybrid and a displaced DNA strand are referred to as R-loops (1).

R-loops are frequently formed during transcription, when the nascent mRNA invades the dsDNA behind the transcribing RNA polymerase. However, R-loops have been detected at sites of DNA double-strand breaks (DSBs) as well as at telomeres, where telomeric repeat-containing non coding RNAs (TERRA), arising from transcription of telomeric regions, frequently hybridize to the complementary telomeric DNA repeats (2). R-loops are also present in the mitochondrial DNA replication origin (3).

The RNA strands in the R-loops are heterogeneous in length, going from few dozens base pairs (bp) to several kb, as well as in sequence, even if they tend to be more frequent in genomic regions characterized by high G-C content (4,5). These RNA–DNA hybrids are widespread along the eukaryotic genome, being found not only in transcribed regions, but also at telomeres, centromeres and enhancers (2,6). Previous studies placed a lower estimate for their abundance in HeLa cells to about 300 R-loops/cell, but also clearly indicated that they are transient in nature with a mean half-life of 11 min. Thus, it can be estimated that cells must resolve tenths of thousand R-loops per day (7).

Such high turnover is ensured by a plethora of factors that are operating in the cells in order to prevent aberrant R-loop formation and remove excessive R-loops. These include transcription factors, RNA processing enzymes, DNA repair and replication accessory proteins and chromatin modifiers (1). Also, several helicases such as Senataxin (8) and RNA helicases of the DEAD-box family, such as DDX1, DDX5, DDX19 and DDX21, are involved in genome-wide R-loops resolution mainly facilitating the unwinding of the RNA strand (9).

The existence of several pathways devoted to the regulation of R-loops formation, along with their high turnover, clearly suggests that cells need to keep a careful balance between formation and resolution of these structures. Indeed, over the years, robust evidence accumulated indicating that R-loops can have both positive and negative effects of cellular homeostasis.

R-loops play important regulatory roles in mitochondrial DNA replication, gene expression, chromatin modifications, immunoglobulin switch recombination (10). They are also essential mediators in the DNA damage response and repair pathways, especially at DSBs and participate in maintaining telomeres integrity (11). On the other side, excessive or deregulated R-loops formation can trigger DNA damage and genome instability, affecting transcription termination, perturbing replication fork progression and causing the accumulation of DSBs. Indeed, R-loops deregulation has been found in several cancer types. In addition, R-loops accumulation can trigger an inflammatory response and defects in R-loops processing factors are linked to pathological conditions such as Aicardi-Goutieres Syndrome and Amyotrophic Lateral Sclerosis, characterized by high levels of chronic inflammation (2,5).

Removal of R-loops is mainly relying on the action of two specialized ribonucleases: RNaseH1 (12–14) and RNaseH2. Human RNaseH1 is a monomeric enzyme, which specifically cleaves RNA–DNA hybrids where the RNA strand is longer than 4 ribonucleotides (rNMPs) (15). RNaseH2 is a trimeric complex formed by the RNaseH2A catalytic and the RNaseH2B and C accessory subunits. Its catalytic properties are different from RNaseH1, most notably in the ability to cleave even a single rNMP embedded in a dsDNA. Thanks to this property, RNaseH2 is the main enzyme carrying out the removal of misincorporated rNMPs during DNA replication or repair, through the Ribonucleotide Excision Repair (RER) pathway (16). However, studies in yeast and human cells have revealed a major role of RNaseH2 also in removing genomic R-loops and suggested a precise spatial and temporal regulation of the activities of RNaseH1 and RNaseH2 (17,18), even if the details of the mechanisms underlying such division of labour are not yet fully understood.

The DEAD-box RNA helicase DDX3X is involved in all aspects of RNA metabolism, but also plays essential roles in cell proliferation and innate immunity pathways. Its deregulation has been linked to neurodegenerative diseases and tumorigenesis (19–22). We have recently shown that DDX3X has RNaseH2-like activity able to operate RER in *in vitro* reconstituted systems. Moreover, we have shown that DDX3X silencing caused accumulation of rNMPs in the cellular genome, supporting its role in removing rNMPs along with RNaseH2 (23).

Given the major role of RNaseH2 in removing R-loops, here we have investigated whether DDX3X could be also involved in R-loops degradation. Using synthetic R-loop mimicking substrates, we could show that human DDX3X alone was able to both displace and degrade the ssRNA strand hybridized to DNA, albeit with lower efficiency with respect to RNaseH2. Moreover, DDX3X was found to physically interact with all three subunits of human RNaseH2. Interaction with the H2B and H2C subunits suppressed the nuclease and helicase activities of DDX3X, but stimulated severalfold the catalytic activity of RNaseH2, but not of RNaseH1. Finally, silencing of DDX3X in human cells caused accumulation of RNA-DNA hybrids and phosphorylated RPA foci. These results support a role of DDX3X as a scaffolding protein and auxiliary factor for RNaseH2 during R-loop degradation.

## Materials and methods

### Proteins production and purification

Human recombinant DDX3X wt was expressed with plasmid pETM41-DDX3X (kindly provided by Dr Nathalie Chamond) and purified from *Escherichia coli* BL21(DE3) cells (Invitrogen) essentially as already described (24). Initially, the plasmid let the production of the fusion protein MBP-TEV-DDX3X that was used for pull-down experiments, while after TEV cleavage, purified DDX3X fractions were pooled, quantified and stored at -80°C (in buffer 20 mM Tris–HCl pH8, 250 mM KCl, 1 mM DTT, 10% glycerol) for the subsequent nuclease and helicase assays.

Representative protein gel and Western blot of the MBP-DDX3X purified fraction used in this study is shown in Supplementary Figures S1A, B.

Human recombinant $DDX3X_{(132–607)}$ and $DDX3X_{DADA}$ (D347A/D350A) mutants were obtained from plasmids pETHis6-MBP-TEV-$DDX3X_{(132–607)}$ and pET30a(+)-$DDX3X_{DADA}$, respectively. Both proteins were purified from *E. coli* BL21(DE3) as previously described (23,25).

Human recombinant RNaseH2 wt complex was purified from *E. coli* MIC1066 cells transformed with plasmid pET-

**Table 1.** Substrates used in this study; RNA nucleotides are in bold

| |
|---|
| Substrate **1** (DNA:**RNA**:DNA) R-loop 15-mer D65:**R15**:D67 |
| 5′-GTACCCGGGGATCCTCTAGAGTCGAGCGTCGATCCGAAACTTGGCACTGGCCGTCGTTTTACAAC-3′ |
| 3′-**CGCAGCUAGGCUUUG**-5′FAM |
| 3′-CATGGGCCCCTAGGAGATCTCACTACTCTAACTCCGACCCTTTTCCGTGACCGGCAGCAAAATGTTG-5′ |
| Substrate **2** (DNA:**RNA**:DNA) R-loop 30-mer D65:**R30**:D67 |
| 5′-GTACCCGGGGATCCTCTAGAGTCGAGCGTCGATCCGAAACTTGGCACTGGCCGTCGTTTTACAAC-3′ |
| 3′-**UCUCAGCUCGCAGCUAGGCUUUGAACCGUG**-5′FAM |
| 3′-CATGGGCCCCTAGGAGATCTCACTACTCTAACTCCGACCCTTTTCCGTGACCGGCAGCAAAATGTTG-5′ |
| Substrate **3** (DNA:DNA**riboC**) dsDNA 55/55**rC** mer D55:D39**R1**D15 |
| 5′-CCAACACACAACACCGTGTGAATTCGGCACTGGCCGTCGTATGCTCTTGGTTGTA-3′ |
| 3′-GGTTGTGTGTTGTGGCACACTTAAGCCGTGACCGGCAGCATACGAGAACCAACAT-5′FAM |

hH2ABC (kindly provided by Dr. Robert Crouch) as described in reference (26).

RNaseH2 double mutant D141N-D169N in the subunit A was sequentially obtained by Gibson assembly (NEB) using primers for mutagenesis (Supplementary Table S1). Then, the RNaseH2 double mutant complex was purified as for the wt complex.

Instead, RNaseH2 subunits B and C were subcloned *Bam*HI–*Xho*I in the plasmid pET28a(+) and purified from *E. coli* BL21(DE3). Briefly, both subunits were induced with 0.4 mM IPTG (Applichem) at 30°C overnight and then purified with a 150–500 mM imidazole (Sigma) gradient from the Ni-NTA resin (Qiagen). Purified fractions were pooled, dialyzed, quantified and stored at −80°C in buffer 50 mM Tris–HCl pH 7.5, 150 mM NaCl, 1 mM DTT, 10% glycerol.

Representative protein gels of the RNaseH2 purified fractions used in this study are shown in Supplementary Figures S1C, D.

Active human recombinant RNaseH1-4892H was purchased from Creative Biomart.

For mammalian transient proteins expression, DDX3X DNA sequence was amplified from pETM41-DDX3X with specific primers (Supplementary Table 1) and cloned in frame EcoRV-NotI in the pHTN-Halotag CMV Neo empty vector (Promega). RNaseH2 subunits and Transglutaminase 2 (TGM2) genes were also amplified from plasmids already available in laboratory with specific primers (Supplementary Table 1) and cloned in frame KpnI-NotI immediately after the NanoLuc in pCMVTnT-NanoLuc vector (Promega) previously modified to contain the NanoLuc reporter sequence at the N-terminus (27). Instead, the DNA sequence that codifies for SARS-CoV-2 nucleoprotein N was subcloned KpnI-NotI from plasmid pCMV3-N codon optimized (SinoBiological) into the pCMVTnT-NanoLuc vector.

## Nucleic acid substrates

RNA oligonucleotides were purchased from Biomers.net GmbH. The sequences of the annealed substrates are summarized in Table 1; bold letters indicate ribonucleotides. For all the substrates, oligonucleotides were mixed in equimolar ratio in annealing buffer (30 mM HEPES–KOH pH 7.4, 100 mM KCl, 2 mM $MgCl_2$, 50 mM $NH_4Ac$) at a final concentration of 500 nM, heated at 95°C for 5 min and then slowly cooled down overnight at room temperature.

## Nuclease assays

The nuclease activity of DDX3X, RNaseH1 and RNaseH2 proteins was analyzed using 50 nM of the different FAM labelled substrates reported in Table 1. Reactions were performed in 20 mM Tris–HCl pH 8.8, 10 mM $(NH_4)_2SO_4$, 10 mM KCl, 2 mM $MgSO_4$, 0.1% TritonX-100 at 37°C. The enzyme concentrations and the time of incubations are indicated in figure legends. Mixtures were stopped by the addition of standard denaturing gel loading buffer (95% formamide, 10 mM EDTA, xylene cyanol and bromophenol blue) and heated at 95°C for 5 min. Finally, reactions were loaded on 7 M urea - 12% polyacrylamide 19:1 gel and run at 40 W for 2 h in 1× TBE buffer. Substrates and products were quantified by laser scanning densitometry at Typhoon-TRIO (GE Healthcare). When DDX3X was used in the presence of RNaseH1 or RNaseH2, proteins were preincubated for 10 min at 4°C before the addition of substrates.

## Non denaturing gel-based helicase assays

The helicase activity of DDX3X wt and mutants and RNaseH2 wt or single subunits was monitored by measuring the conversion of 50 nM of substrate 1 (Table 1) into a 15 mer FAM labelled single strand RNA. Reactions were performed in helicase buffer (20 mM Tris–HCl pH 8, 2 mM DTT, 70 mM KCl, 2 mM $MgCl_2$, 6U RNasin) and started with the addition of 4 mM ATP. After 30 min of incubation at 37°C, reactions were stopped by adding 6× gel loading buffer (Thermofisher) and run on 10% TBE-polyacrylamide 19:1 + 0.1% SDS gel at 40V for about 3 h in 1× TBE + 0.1% SDS buffer at 4°C in mini-PROTEAN electrophoresis system (Bio-Rad). Substrates and products were quantified by laser scanning densitometry at Typhoon-TRIO. When DDX3X was used in the presence of RNaseH2, proteins were preincubated for 10 min at 4°C before the addition of substrate 1 and ATP.

## Pull-down assay

Cellular pull-down assay was initially carried out using the Halotag mammalian pull-down system (Promega) following manufacturer's instructions with few modifications. Human U2OS cells were seeded in a 10 cm cell culture dish and transfected at 90% of confluence with 10 μg of plasmid pHTN-Halotag-DDX3X using lipofectamine 2000 (Invitrogen). After 48 h, cells were washed in PBS 1×, lysed with 300 μl of PLB 1× buffer (Promega) containing Sigmafast protease inhibitor cocktail (Sigma) and centrifuged for 10 min at 10 000 rpm at 4°C. Clarified lysate was incubated with 50 μl of pre-equilibrated HaloLink resin (Promega) for 3 h at 25°C in agitation. Then, resin was washed four times with 500 μl of TBST 1× buffer and incubated with 50 μl of TEV buffer 1× + 1 mM DTT + 25U TEV plus protease (Promega) for 1 h at 25°C in agitation. Next, TEV treated supernatant was recovered and RNaseH2 pull-down was verified in Western blot. Control

experiment was performed with U2OS cell lysate transfected with the pHTN-Halotag CMV neo empty vector.

Luminescent pull-down assay was also a modification of the Halotag mammalian pull-down system. 0.5 × $10^6$ of human U20S cells were seeded in 6-well plate and transfected the next day using lipofectamine 2000 with 3 μg of plasmid to express Halo-DDX3X or the NanoLuc fusion proteins. After 48 h cells were lysed in 300 μl of PLB 1× buffer containing Sigmafast protease inhibitor cocktail and centrifugated at 10 000 rpm for 10 min. Clear lysates were checked for transfection efficiency verifying the light units (LU) of the NanoLuc expressed proteins with Nano-Glo Luciferase Assay (Promega) in GloMax luminometer (Promega) and by Western blot with anti-NanoLuc Abs (Supplementary Figure S2A), while Halo-DDX3X expression was verified with Halotag TMR ligand and quantified in Western blot using a purified DDX3X protein as standard. Then, luminescent pull-down assays were performed by mixing 3 μg of Halo-DDX3X protein with the same LU amount of NanoLuc tagged proteins and 50 μl of pre-equilibrated HaloLink resin to reach a total volume of 500 μl in TBST 1× with the addition of 20 μg/ml DNaseI (Merck Millipore) and of 100 μg/ml RNase (Roche). Samples were incubated for 3 h at 25°C in agitation, then the HaloLink resin was washed four times with TBST 1× and incubated with 50 μl of TEV buffer 1× + 1 mM DTT + 10U TEV plus protease for 1 h at 25°C in agitation. Finally, luminescence was calculated in sample supernatants using the Nano-Glo Luciferase Assay.

*In vitro* pull down assays to verify the interaction between MBP-DDX3X with RNaseH2 using *E. coli* expressed recombinant proteins were performed using a similar procedure. MBP-DDX3X protein was expressed in BL21(DE3) *E. coli* cells resuspended in buffer A (50 mM Tris pH 8, 150 mM NaCl, 0.05% NP40) and lysed by adding lysozyme 10 mg/ml, 1 mM EDTA and Sigmafast protease inhibitor cocktail. After sonication and centrifugation at 20 000 rpm for 30 min, the clear cell lysates corresponding to 10 μg of MBP-DDX3X protein was bound to 30 μl of MBP resin Amintra (Abcam) in the presence of 20 μg/ml of DNaseI and incubated for 4 h at 4°C at 850 rpm on Thermomixer HC (Starlab). Then, after extensive washing with 1× PBS, 10 μg of recombinant RNaseH2 complex or RNaseH2 subunits B or C were diluted to 150 μl in buffer A, added to the resin and incubated overnight at 16°C on Thermomixer HC. The following day, the supernatant was discarded, the resin washed with 1× PBS and treated with 10 U of TEV protease (Promega) in 150 μl of buffer A plus 1 mM DTT for 2 h at 25°C in agitation. Finally, the supernatant was recovered and the collected samples were analyzed in Western blot. Control experiments were carried out by using BL21(DE3) cell lysate transformed with pETHis6-MBP-TEV empty 29656 vector (Addgene).

## Cell cultures

U2OS and A549 cells were grown in high-glucose DMEM supplemented with 10% FBS and 1% penicillin/streptomycin.

Cells were regularly tested and verified to be negative for mycoplasma before experiments.

## Western blotting

Western blot analysis was performed according to standard procedures. Protein samples were separated by 10% SDS-PAGE, blotted onto 0.2 μm Amersham Protran nitrocellulose membrane (GE Healthcare) and incubated overnight with primary antibodies: 1:1000 rabbit polyclonal anti-DDX3X A300-474A (Bethyl), 1:1000 rabbit polyclonal anti-RNaseH2A ab83943 (Abcam), 1:1000 rabbit polyclonal anti-RNaseH2B ab122619 (Abcam), 1:1000 rabbit polyclonal anti-RNaseH2C HPA065375 (Sigma), 1:1000 Anti-NanoLuc monoclonal antibody (Promega) and 1:1000 mouse monoclonal anti-Vinculin MAB3574 (Millipore). The day after, membranes were incubated for 1 h with HRP-conjugated secondary antibodies goat anti-rabbit or goat anti-mouse (1:5000) (Sigma) and chemiluminescent signals were developed using the ECL reagent Westar Nova 2.0 (Cyagen) and Chemidoc imaging system (Bio-Rad).

## Small-interfering RNA transfections

All siRNAs were purchased from Dharmacon™-Horizon Discovery and were transfected using RNAiMAX (Invitrogen) according to manufacturer instructions. siRNAs were used at final concentration of 5 nM for DDX3X (ON-TARGETplus Human DDX3X siRNA, SMARTPool), 20 nM for RnaseH2A (ON-TARGETplus Human RNASEH2A siRNA, SMARTPool), 20nM for RNaseH2B (ON-TARGETplus Human RNASEH2B siRNA, SMARTPool). As negative control was used Non-Targeting siRNAs pool (ON-TARGETplus Non-targeting Control Pool). Silencing efficiency was tested by Western blotting using rabbit polyclonal anti-DDX3X A300-475A, rabbit polyclonal anti-RNaseH2B ab122619 (Abcam) and mouse monoclonal anti-Vinculin antibody as described above (Supplementary Figure S2B).

1 × $10^5$ cells were plated into six multiwell plates and grown at 37°C at 5% of $CO_2$ in order to obtain 70–80% of confluency after 72 h. For Dot-blot assay after 72 h cells were trypsinized and DNA was extracted as described below; for immunofluorescence cells were plated and silenced directly on coverslip and after 72 h fixed and processed as described below.

## Dot-blotting with S9.6 antibody

Nucleic acids were analysed by Dot-blot as previously described (28) with some modifications; briefly we started from 2.5 × $10^6$ cultured U2OS cells and to extract nucleic acids, we followed the cultured cells protocol listed in the NucleoSpin Tissue DNA kit from Macherey-Nagel. A fraction of the samples was digested with RNaseIII plus RNaseH, or RNaseH alone to hydrolyze RNA bound to DNA and served as a control for the specific detection of RNA-DNA hybrids. We used 1U of RNaseIII (AM2290; ThermoFisher Scientific) per μg of genomic DNA for 2 h at 37°C and 10 U of RNaseH (M0297; NEB) per μg of DNA O/N at 37°C. Serial dilutions of each sample was spotted directly on a positively charged Nylon membrane Hybond™-N+ (Amersham) using a Dot-blot apparatus (Biorad) and immediately crosslinked unto the membrane at an energy of 1, 200 mJ x 100/$cm^2$. DNA was probed with the 1:1000 mouse anti-S9.6 primary antibody (purified from hybridoma cell line kindly provided by Dr. Simone Sabbioneda) at 4°C O/N after saturating the membrane with 5% milk. The day after, membranes were incubated for 1 h with HRP-conjugated secondary antibodies goat anti-mouse (1:5000) (Sigma) and chemiluminescent signals were developed using the ECL reagent Westar Nova 2.0 (Cyagen) and Chemidoc imaging system (Bio-Rad). Images were quantified

using ImageJ software (https://imagej.nih.gov/ij/). Membranes were stripped using a Mild Stripping buffer pH 2.2 (15 g glycine, 1 g SDS, 10 ml Tween20 for 1L of solution); membranes were washed twice with stripping buffer 10 min at room temperature, twice with PBS 1× for 10 min and twice with TBST 1× for 5 min and then saturated with 5% milk. After that membranes were probed with the 1:500 mouse anti-dsDNA primary antibody (HYB331-01; Santa Cruz) O/N at 4°C. The day after membranes were incubated and developed as described above.

### Immunofluorescence assays

Immunofluorescences (IF) were performed as previously described (29) with some modifications. Briefly all cell culture samples were grown, fixed, washed, enzymatically treated, immunostained, and imaged in six multiwell dishes. Cells were fixed with 2 ml of ice-cold, 100% methanol for 10 min at −20°C and then were washed once with PBS 1× before subsequent preparation steps for IF. Samples were then incubated in staining buffer (TBST with 0.1% BSA [A9647-50G; Sigma-Aldrich]) for 30 min with rocking. Enzymatic treatments were done in staining buffer supplemented with 3 mM magnesium chloride with 1:200 dilutions of RNaseT1 (EN0541; ThermoFisher Scientific), RNaseIII (AM2290; ThermoFisher Scientific) and RNaseH (M0297; NEB) and incubated for 1 h at room temperature. For primary immunolabeling, samples were incubated in staining buffer with 1:500 dilutions of mouse S9.6 and rabbit anti-Phospho RPA32 (S4/S8) (A300-245A; Bethyl). Primary antibody were incubated O/N at 4°C. Samples were then washed once with staining buffer and incubated with 1:400 dilutions of secondary Goat anti-rabbit Alexa Fluor Plus 488 conjugate (A32731; Invitrogen) for Phospho RPA32 (S4/S8) and Goat anti-mouse Alexa Fluor Plus 647 conjugate (A32728; Invitrogen) for S9.6 for 1h at room temperature. After one wash with 1× TBST, coverslips were incubated with 1 μg/ml DAPI/1× PBS for 15 min in dark at RT. Then the coverslips were washed twice with 1× TBST and mounted with Aqua-Poly/Mount (18606-20; Polysciences).

### Imaging and image analysis

Immunofluorescence images were acquired using a Confocal Laser Scanning Microscope (Zeiss LSM-800) equipped with 4 lasers: Diode laser 405 nm (5mW); Diode laser 488 nm (10mW); Diode laser 561 nm (10 mW); Diodo laser 640 nm (5 mW), two Master gain with high sensitivity and a 63× 1.4Na objective. For each experiment, all conditions were imaged in parallel, with identical exposure times and laser settings. Images were analyzed and quantified using ImageJ/Fiji and Cell Profiler 4.1.3. Nuclear mean S9.6 and Phospho RPA32 (pRPA) intensities were determined from a single plane for individual images (projection type Sum Slices). Nuclear regions were defined by masking DAPI.

### Quantification and statistical analysis

Statistical analysis was performed with GraphPad Prism 6.01 software using two-tailed unpaired Student's t test. Statistical details of experiments can be found in the figure legends.

## Results

### Both human DDX3X and RNaseH2 can process synthetic R-loops.

We have previously shown that human DDX3X RNA helicase possesses RNaseH2-like activity (23). We then asked whether DDX3X was able to process also R-loops, similarly to RNaseH2. To this aim, DDX3X was incubated in the presence of Substrate **1** (Table 1) mimicking a R-loop structure, whose 15-mer RNA strand was 5′-labelled with a fluorescence group. Digested products were resolved on a sequencing gel. A shown in Figure 1A, DDX3X was able to progressively digest the RNA strand down to di- and mononucleotides, with a strong pausing site around the middle of the strand (Figure 1A, lanes 2–6). RNaseH2, when tested on the same substrate, was also able to digest the RNA strand, but with a clearly different patterns, leading to the accumulation of discrete products of sizes ranging from 6 to 10 nt, which were not changed either upon increasing the enzyme concentration or the incubation time. (Figure 1B, lanes 2–11).

### Exonucleolytic versus endonucleolytic R-loop digestion by DDX3X and RNaseH2.

Overall, the digestion pattern of DDX3X shown in Figure 1A was suggestive of an exonucleolytic mode of action, while RNaseH2 behavior as shown in Figure 1B was more consistent with an endonucleolytic mechanism. In order to confirm these observations, DDX3X and RNaseH2 activities were compared on R-loop Substrate **1** and on Substrate **2** bearing a longer (30-mer) RNA strand. Again, DDX3X was able to digest both R-loops down to mononucleotides (Figure 1C, lanes 3 and 11), while RNaseH2 generated a series of discrete products never shorter than 6 nt (Figure 1C, lanes 2 and 12). However, about a 250- fold higher concentration of DDX3X with respect to RNaseH2 were required to attain a comparable digestion (Figure 1C, compare lanes 2 and 12 with lanes 3 and 11), indicating a greater specificity of RNAseH2 for R-loops, with respect to DDX3X.

The cut sites of RNaseH2 on both the 15- and 30-mer RNA strands are reported in Figure 1D. The products accumulating in Figure 1C were generated through cutting sites always close to rG/dC or rC/dG basepairs, which may represent pausing sites. This is consistent with the previous observation that RNaseH2 digestion of a single rNMP embedded in DNA is slower for rG/dC and rC/dG basepairs than for rA/T or rU/dA (30). In addition, on both substrates the size of the digested products was limited to 5–6 nt downstream the 5′ end and upstream the 3′ end of the RNA strand, suggesting that RNAseH2 requires a RNA:DNA hybrid of at least 5–6 nt for stable binding. RNaseH2 was unable to digest ssRNA, consistent with its substrate specificity for RNA-DNA hybrids. On the other hand, DDX3X was able to completely digest both the 15- and 30-mer ssRNAs, generating a clear exonucleoytic ladder of products (Figure 1C, lanes 6–8 and 14–16). Overall, these data indicate an exonucleolytic versus endonucleolytic R-loop digestion mechanism by DDX3X vs. RNaseH2, respectively.

### DDX3X stimulates RNaseH2 digestion of R-loops

When DDX3X was tested in combination with RNaseH2, a clear increase of activity was detected on both Substrates **1** and **2**, but with a digestion pattern identical to the one of

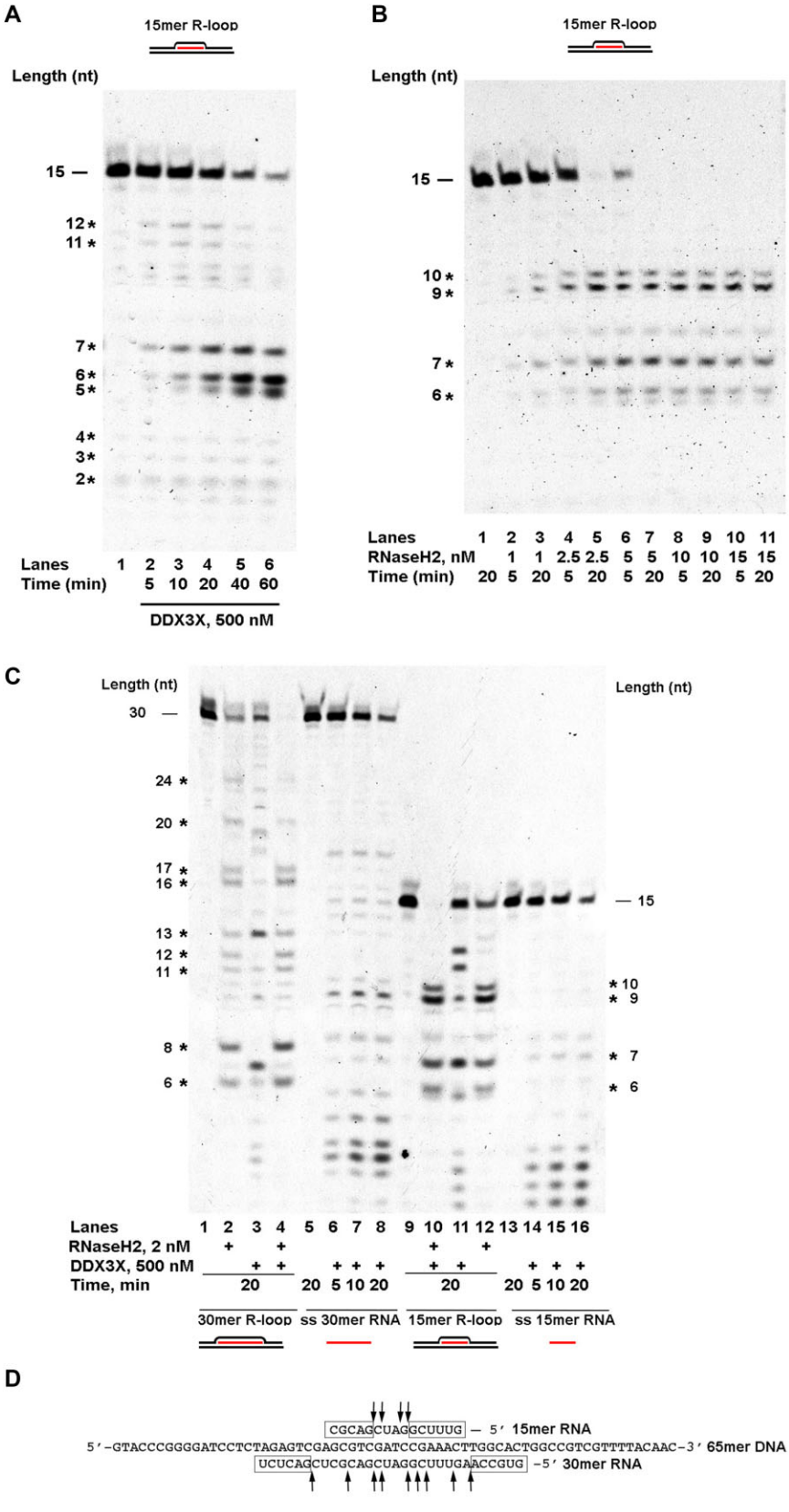


**Figure 1.** RNaseH2 and DDX3X process R-loops with different digestion patterns. (**A**) Time course of recombinant human DDX3X incubated in the presence of substrate 1. Lane 1, control reaction in the absence of DDX3X. (**B**) Increasing concentrations of recombinant human RNaseH2 were incubated for the indicated times in the presence of substrate 1. Lane 1, control reaction in the absence of RNaseH2. (**C**) Comparison of the nuclease activities of DDX3X (lanes 3, 4, 10, 11) and RNaseH2 (lanes 2, 4, 10, 12) either alone or in combination, on the synthetic R-loop substrates 1 (lanes 10–12) and 2 (lanes 2–4), and of DDX3X alone on the 15-mer (lanes 14–16) and 30-mer (lanes 6–8) ssRNA substrates. Lanes 1, 5, 9, 13, control reactions in the absence of enzymes. In all panels, asterisks indicate the major digested products along with the respective nt lengths. (**D**) Schematic diagram of the major cut sites, indicated by arrows, of RNaseH2 on the RNA strand of substrates 1 (top) and 2 (bottom).

RNaseH2 alone (Figure 1C, compare lanes 2 and 12 with lanes 4 and 10). In order to further characterize this effect, increasing amounts of DDX3X were titrated in the absence or in the presence of a fixed amount of RNaseH2 on Substrate **1** (Figure 2A). At the concentration tested of 2 nM, RNaseH2 alone digested approx. 20% of the substrate (Figure 2A, lane 2 and Figure 2C). In agreement with the previous observations, DDX3X alone showed a similar activity only at 200 nM (Figure 2A, lane 7 and Figure 2C), while at the highest concentration tested (500 nM), was able to digest approx. 50% of the substrate (Figure 2A, lane 8 and Figure 2C). However, combination of 2 nM RNaseH2 with 10 nM DDX3X showed a dramatic increase in activity, leading to the digestion of >70% of the substrate and reaching near complete digestion already at 50 nM DDX3X (Figure 2A, lanes 9–13 and Figure 2C). Again, the digestion pattern was identical to the one shown by RNaseH2 alone. Only at the highest DDX3X concentration, additional shorter products appeared (Figure 2A, lane 14). When the incubation time was raised from 20 to 40 min, significant stimulation of 2 nM RNaseH2 activity was observed already in the presence of 1 nM DDX3X, reaching near complete digestion of the substrate at 10 nM DDX3X (Figure 2B, compare lane 3 with lanes 7, 8), while 1 nM DDX3X alone did not show any detectable nuclease activity (Figure 2B, lane 4). By plotting the increase in digested product with respect to RNaseH2 alone, as a function of the DDX3X concentration, an apparent affinity constant for the functional RNaseH2-DDX3X interaction of 5.7 nM was obtained (Figure 2D).

Overall, these results confirmed that DDX3X was able to stimulate RNaseH2 processing of R-loops *in vitro*, even at concentrations at which DDX3X alone did not show any nuclease activity.

## DDX3X stimulates processing of a single rNMP embedded in DNA by RNaseH2

When DDX3X was tested in combination with a limiting amount of RNaseH2 on a dsDNA substrate containing a single embedded rNMP (Figure 3A, lanes 9–14), a significant stimulation of rNMP digestion was observed, with respect to the activity of RNaseH2 alone (Figure 3A, lane 2) or DDX3X alone (Figure 3A, lanes 3–8). At the concentration tested of 2 nM, RNaseH2 alone digested approx. 20% of the substrate, while DDX3X at lowest concentration tested of 20 nM, processed <10% of the substrate. When assayed in combination, however, about 90% of the substrate was processed, indicating a strong synergistic effect (Figure 3B). By plotting the increase in digested product with respect to RNaseH2 alone, as a function of the DDX3X concentration, an apparent affinity constant for the functional RNaseH2-DDX3X interaction of 6.7 nM was obtained (Figure 3C), in agreement with the results obtained on the synthetic R-loop substrates (Figure 2D).

Thus, DDX3X was able to act synergistically with RNaseH2 also in the removal of single rNMPs embedded in dsDNA.

## Stimulation of RNaseH2 activity does not depend on the nuclease activity of DDX3X

DDX3X alone can process both R-loops (Figure 1A) and single rNMPs embedded in dsDNA (Figure 3A lanes 3–8 and 23). In order to test whether such nuclease activity was responsible for the synergistic effect of its combination with RNaseH2, a the $DDX3X_{(132–607)}$ mutant carrying a deletion of the first 131 N-ter and of the last 54 C-ter aminoacids was assayed. We have previously shown that the $DDX3X_{(132–607)}$ mutant was devoid of nuclease activity of single rNMPs (23). When tested in the presence of the synthetic R-loop Substrate **1**, this mutant showed complete absence of nuclease activity as well (Figure 3D, lanes 5, 6). However, when combined with a limiting amount of RNaseH2, a strong stimulation of R-loop digestion was observed (Figure 3D, lanes 7, 8), with respect to RNaseH2 alone (Figure 3D, lane 2). Similarly, the $DDX3X_{(132–607)}$ mutant was completely inactive on the dsDNA substrate containing a single embedded rNMP as expected (Figure 3E, lanes 5, 6), but still able to stimulate RNaseH2 activity (Figure 3E, compare lane 2 with lanes 5, 6). It was noted that the stimulation of the RNaseH2 activity on the R-loop substrate by the $DDX3X_{(132–607)}$ mutant was apparently lower in magnitude than the one observed with the single rNMP substrate (compare lanes 7 and 8 of Figure 3D, with the same lanes of Figure 3E). It is possible that due to the missing N- and C-ter domains, the $DDX3X_{(132–607)}$ mutant may have a slightly weaker interaction with the particular structure of the R-loop substrate, dissociating faster than from the linear dsDNA containing a single rNMP.

Collectively, these results indicate that the nuclease activity of DDX3X was not required for the stimulation of RNaseH2.

## DDX3X helicase activity can displace R-loops independently from its nuclease activity and is inhibited by RNaseH2

When tested in a helicase assay on the synthetic R-loop Substrate **1**, DDX3X was able to displace the RNA strand in an ATP-dependent manner (Figure 4A, lanes 2–4). However, combination of DDX3X with RNaseH2 resulted in a significant inhibition of the helicase activity on Substrate **1** (Figure 4B, compare lanes 3–5 with lanes 6–8). As expected, RNaseH2 alone did not show any helicase activity on this substrate (Figure 4B, lane 2). In order to test whether the nuclease activity of DDX3X was involved in the displacement of the R-loop, the experiment shown on Figure 3B was replicated in the presence of the $DDX3X_{(132–607)}$ mutant, which is devoid of any nuclease activity, but retains full helicase activity (23). Similarly to what was observed with wt DDX3X, the $DDX3X_{(132–607)}$ mutant was able to displace the RNA strand from the synthetic R-loop Substrate **1** (Figure 4C, lanes 3–5) and its helicase activity was inhibited by RNaseH2 (Figure 4C, lanes 6–8).

Overall, these results indicate that DDX3X can act as a RNA helicase on R-loops, independently from its nuclease activity, and that its helicase activity is inhibited by RNaseH2.

## Stimulation of RNaseH2 activity does not depend on the helicase activity of DDX3X

In order to better assess whether the helicase activity of DDX3X was somehow involved in the stimulation of RNaseH2, the $DDX3X_{(DADA)}$ mutant was tested. This mutant, carries two Asp→Ala substitutions in the aspartic acids of the Walker B motif D-E-A-D, completely lacking ATPase and helicase activities (31). As expected, when tested on the synthetic R-loop Substrate **1**, the $DDX3X_{(DADA)}$ mutant was unable to displace the RNA strand either alone (Figure 4D, lanes 3–5), or in combination with RNaseH2 (Figure 4D, lanes 6–8). However, when tested on the same substrate in a nuclease assay, the $DDX3X_{(DADA)}$ mutant was able to stimulate the RNaseH2 activity at levels comparable to wt DDX3X and

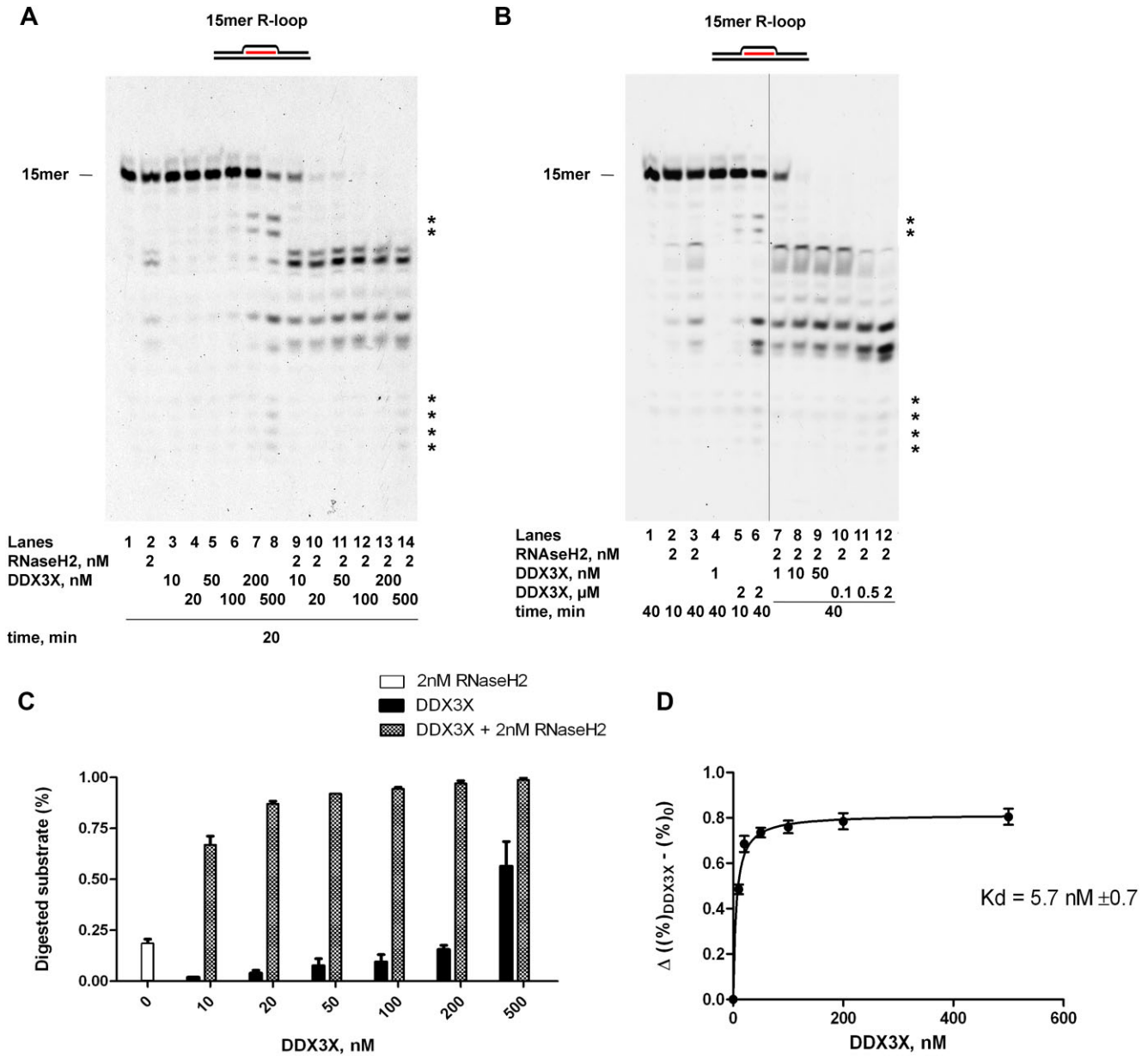


**Figure 2.** Stimulation of R-loop processing activity of RNaseH2 by DDX3X. (**A**) Increasing concentrations of human recombinant DDX3X were incubated with substrate 1, either alone (lanes 3–8) or in combination with a fixed dose of human recombinant RNaseH2 (lanes 9–14). Lane 1, control reaction in the absence of enzymes; Lane 2 control reaction with RNaseH2 alone. Asterisks indicate relevant digestion products as discussed in the text. (**B**) Increasing concentrations of DDX3X were incubated with a fixed amount of RNaseH2 on substrate 1 (lanes 7–12). Lane 1, control reaction in the absence of enzymes; Lanes 2–3 control reactions with RNaseH2 alone; Lanes 4–6 control reactions with DDX3X alone. Asterisks indicate relevant digestion products as discussed in the text. (**C**) Quantification of the digested substrate by a fixed amount of RNaseH2 alone (white bar), increasing amounts of DDX3X alone (black bars) or their combination (grey bars). Values are the mean of two independent experiments. Error bars indicate ± S.E. (**D**) Increase in the RNaseH2 digestion activity from panel C was plotted as a function of DDX3X concentrations. Data were fitted to Eq. (1) to derive the apparent dissociation constant for DDX3X-RNaseH2 interaction. Values are the mean of two independent experiments. Error bars indicate ± S.E.

the DDX3X$_{(132–607)}$ mutant (Figure 4E, compare lanes 4 and 6 with lane 8).

Collectively, these results indicate that the helicase activity of DDX3X is not required for the stimulation of RNaseH2 activity on R-loops.

## DDX3X physically interacts with RNaseH2

Since the stimulation of RNaseH2 activity was independent from both the helicase and nuclease activities of DDX3X, a physical interaction between the two proteins was investigated. To this aim, a pull-down assay using purified proteins was performed. Recombinant MBP-tagged DDX3X was loaded on the corresponding affinity beads and incubated with either the human trimeric RNaseH2, or with the single purified H2B and H2C subunits of RNaseH2. Bound proteins were eluted by digestion with the TEV protease and revealed by Western blot with specific antibodies. Upon incubation of MPB-DDX3X with heterotrimeric RNaseH2, elution by TEV digestion allowed the recovery of the entire RNaseH2 complex as revealed by Western blot with antibodies specific for each subunit (Figure 5A–C). Similarly, when MPB-DDX3X

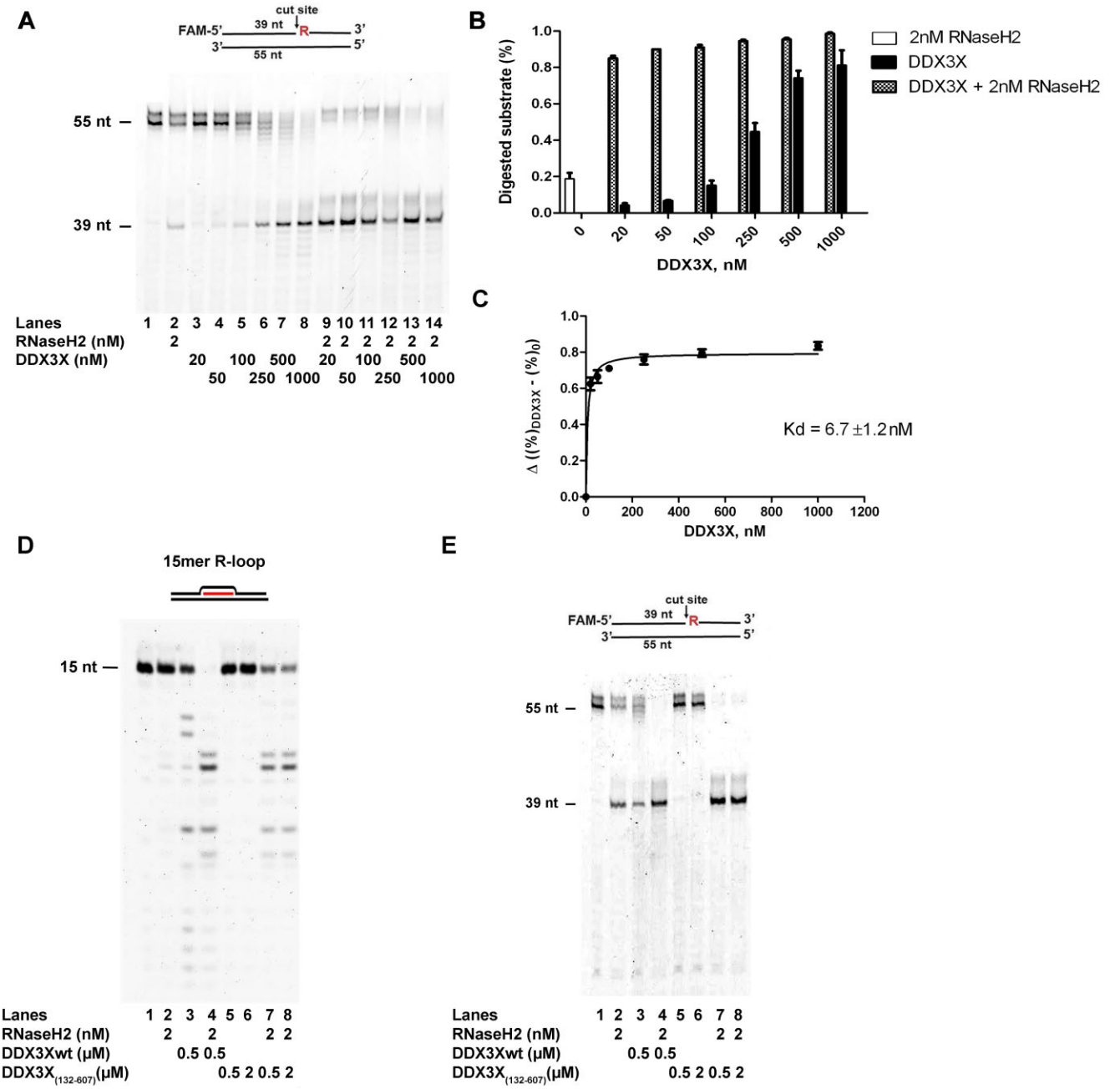


**Figure 3.** DDX3X stimulates RNaseH2 independently from its ribonuclease activity. (**A**) Increasing concentrations of human recombinant DDX3X were incubated with substrate 3, either alone (lanes 3–8) or in combination with a fixed dose of human recombinant RNaseH2 (lanes 9–14). Lane 1, control reaction in the absence of enzymes; Lane 2 control reaction with RNaseH2 alone. (**B**) Quantification of the digested substrate by a fixed amount of RNaseH2 alone (white bar), increasing amounts of DDX3X alone (black bars) or their combination (grey bars). Values are the mean of two independent experiments. Error bars indicate ± S.E. (**C**) Increase in the RNaseH2 digestion activity from panel B was plotted as a function of DDX3X concentrations. Data were fitted to Eq. (1) to derive the apparent dissociation constant for DDX3X-RNaseH2 interaction. Values are the mean of two independent experiments. Error bars indicate ± S.E. (**D**) RNaseH2 was incubated on substrate 1 either alone (lane 2), or in combination with DDX3Xwt (lane 4) or the $DDX3X_{(132–607)}$ deletion mutant (lanes 7, 8). Lane 1, control reaction in the absence of enzyme; Lane 3 control reaction with DDX3Xwt alone; Lanes 5, 6, control reactions with $DDX3X_{(132–607)}$ alone. (**E**) As in panel D but in the presence of substrate 3.

was incubated separately with the single H2B and H2C subunits, both subunits co-eluted with DDX3X upon TEV digestion (Figure 5D and E).

A different pull-down approach was also performed using U2OS cells transiently transfected to express Halo-DDX3X protein. This version of DDX3X was captured on HaloLink resin and bound proteins were eluted with TEV digestion. Western blot analysis revealed that cellular RNaseH2 interacted with DDX3X (Figure 6A). To further investigate these interactions, a pull-down assay was also developed based on NanoLuc tagged RNaseH2 subunits expressed in cells. Halo-DDX3X expressed in U2OS cells was captured on Halolink resin together with the different NanoLuc RNaseH2 subunits and luminescent signals were measured after TEV treatment. The strength of interaction was proportional to the luminescence signal. All the three recombinant

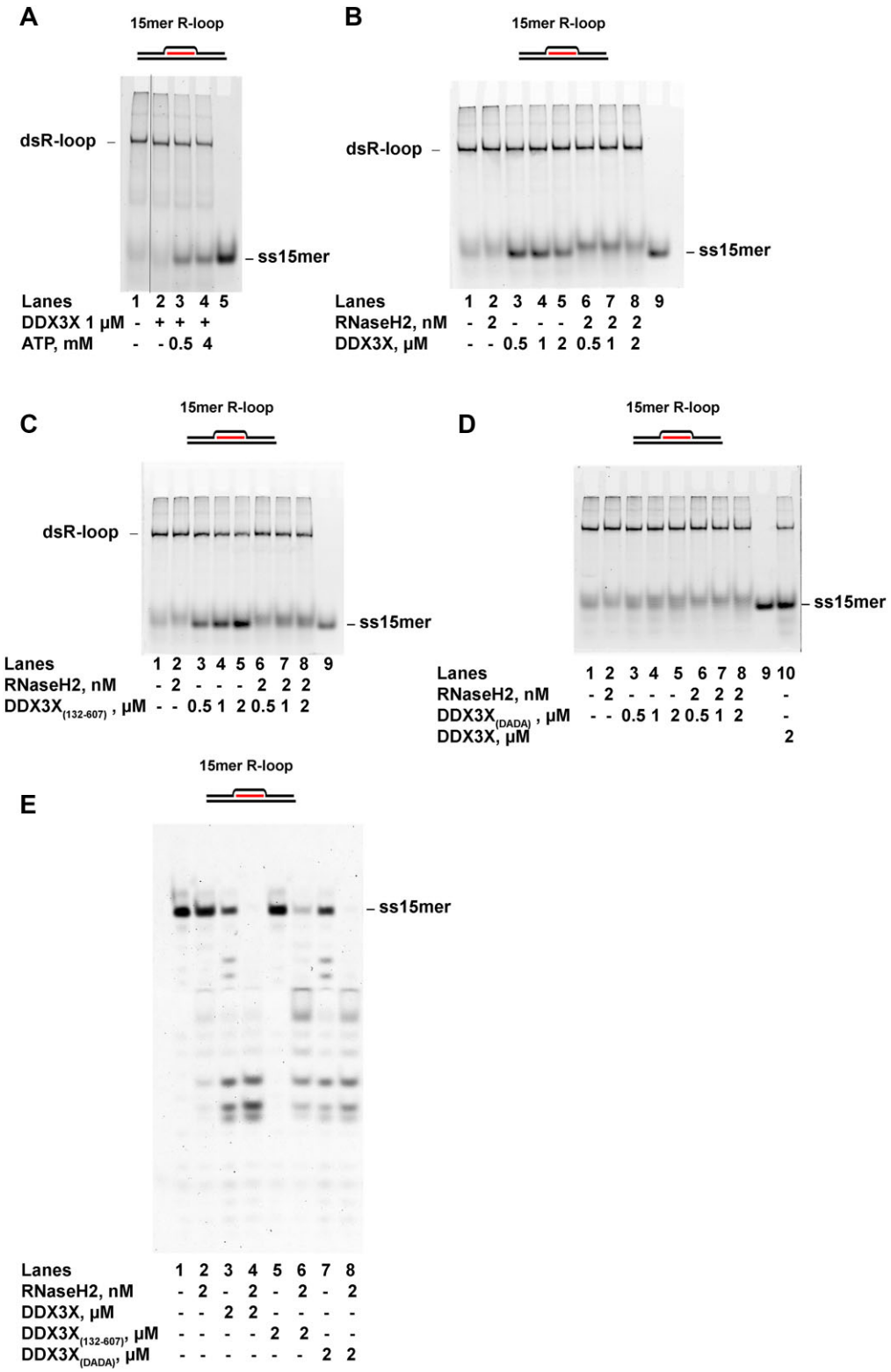


**Figure 4.** DDX3X helicase activity on R-loops is inhibited by RNaseH2 and is dispensable for its stimulation. (**A**) Helicase activity of DDX3X on substrate 1 in the absence (lane 2) or in the presence (lanes 3, 4) of ATP. Lane 1, control reaction in the absence of DDX3X; Lane 5, 15-mer ssRNA strand alone as marker for the displaced products. (**B**) Increasing amounts of DDX3X were titrated in a helicase assay on substrate 1, either alone (lanes 3–5) or in combination with a fixed amount of RNaseH2 (lanes 6–8). Lane 1, control reaction in the absence of enzymes; Lane 2, control reaction with RNaseH2 alone, Lane 9, 15-mer ssRNA strand alone as marker for the displaced products. (**C**) As in panel B, but in the presence of the $DDX3X_{(132–607)}$ deletion mutant. (**D**) As in panel B, but in the presence of $DDX3X_{(DADA)}$ mutant. (**E**) Nuclease activity of DDX3Xwt and mutants either alone (lanes 3, 5, 7) or in combination with RNaseH2 (lanes 4, 6, 8). Lane 1, control reaction in the absence of enzymes; Lane 2, control reaction with RNaseH2 alone.

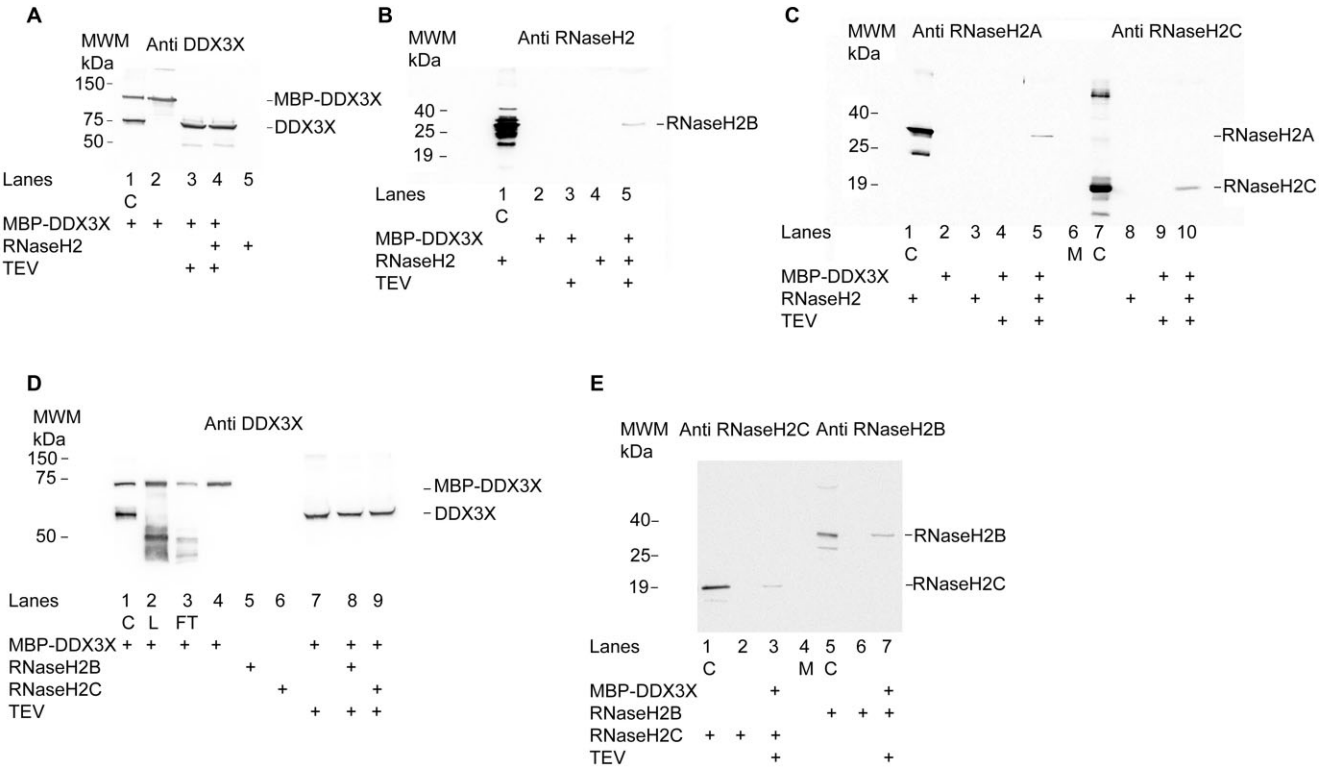


**Figure 5.** DDX3X physically interacts with the RNaseH2 trimeric complex in an *in vitro* assay. (**A**) MBP-tagged DDX3X was incubated with the affinity beads either alone (lanes 2–3) or with human recombinant RNaseH2 (lane 4). Bound proteins were eluted by TEV digestion (lanes 3, 4) and analyzed by Western blot with anti-DDX3X Abs. Lane 1, positive control mixture for purified MBP-DDX3X and DDX3X.; Lane 5, control beads incubated with RNaseH2 alone. (**B**) Same samples of panel A but analyzed by Western blot with anti-RNaseH2B Abs. Lane 1, positive control for RNaseH2B; Lanes 4, affinity beads incubated with RNaseH2 alone; Lane 5, affinity beads incubated with MBP-DDX3X and RNaseH2 and eluted by TEV digestion. (**C**) Same samples of panel A and B but analyzed by Western blot with anti-RNaseH2A (lanes 1–5) or anti RNaseH2C (lanes 7–10) Abs. Lanes 1, 7, positive controls for RNaseH2 A and C; Lanes 5, 10, affinity beads incubated with MBP-DDX3X and RNaseH2 and eluted by TEV digestion. (**D**) MBP-tagged DDX3X was incubated with the affinity beads either alone (lanes 4, 7) or with human recombinant RNaseH2B or RNAseH2C subunits (lanes 8–9). Proteins were eluted by TEV digestion (lanes 7–9) and analyzed by Western blot with anti-DDX3X Abs. Lane 1, positive control mixture for purified MBP-DDX3X and DDX3X, Lane 2, input loaded on MBP affinity beads. Lane 3, flow-through; Lanes 5 and 6, control beads incubated with RNaseH2B or H2C alone. (**E**) Western blot with anti RNaseH2C (lanes 1–3) or anti RNaseH2B (lanes 5–7) Abs of the corresponding samples shown in panel D. Lanes 1, 5, positive controls for RNaseH2 B and C subunits.

NanoLuc tagged RNaseH2 subunits, including the H2A mutant D141N-D169N, were found to bind DDX3X. Interaction between DDX3X and SARS-CoV-2 N protein was used as positive control (32), while no signals were obtained with NanoLuc-TGM2 or NanoLuc, only used as negative controls (Figure 6B).

Collectively, these results indicated that DDX3X physically interacted with all subunits of the RNaseH2 trimeric complex.

## The B and C subunits of RNaseH2 inhibit the DDX3X nuclease and helicase activities on R-loops

Human RNaseH2 is a heterotrimeric protein composed by the catalytic subunit H2A and the two accessory subunits H2B and H2C (26). Since all three subunits physically interacted with DDX3X (Figure 6), in order to determine whether the B and C subunits were involved in the modulation of DDX3X activities on R-loop, both were expressed separately and tested in either nuclease or helicase assays on the synthetic R-loop Substrate **1**. As expected, neither subunit alone showed nuclease activity (Figure 7A, lanes 2, 3). DDX3X, on the other hand, was able to digest the RNA strand (Figure 7A, lane 4). However, a dose-dependent reduction of digested products was observed when a fixed concentration of DDX3X was tested in the presence of increasing amounts of H2B (Figure 7A, lanes 5–7) or H2C (Figure 7A, lanes 8–10). Simultaneous addition of H2B and H2C in the absence of DDX3X also did not result in any nuclease activity on the synthetic R-loop Substrate **1**. (Figure 7B, lanes 4–6). However, when increasing equimolar amounts of both H2B and H2C were added to the reaction in the presence of a fixed concentration of DDX3X, a strong reduction of digested products with concomitant accumulation of the undigested 15-mer RNA strand was observed with respect to DDX3X alone (Figure 7B, compare lane 7 with lanes 8–10).

When tested in helicase assays on the synthetic R-loop Substrate **1**, H2B or H2C were not able to displace the 15-mer RNA strand either alone (Figure 7C and D, lane 3) or in combination (Figure 7E, lanes 3–5). As expected, DDX3X alone efficiently displaced the 15-mer RNA strand (Figure 7C and E, lane 2). However, when DDX3X was tested in the presence of H2B or H2C alone (Figure 7C and D, lanes 4–8), or in combination (Figure 7E, lanes 6–8), almost complete inhibition of the helicase activity was observed, as indicated by the strong reduction of the displaced 15-mer RNA strand.

Collectively, these results indicated that the RNaseH2 subunits H2B and H2C negatively modulated both catalytic activities of DDX3X on R-loops.

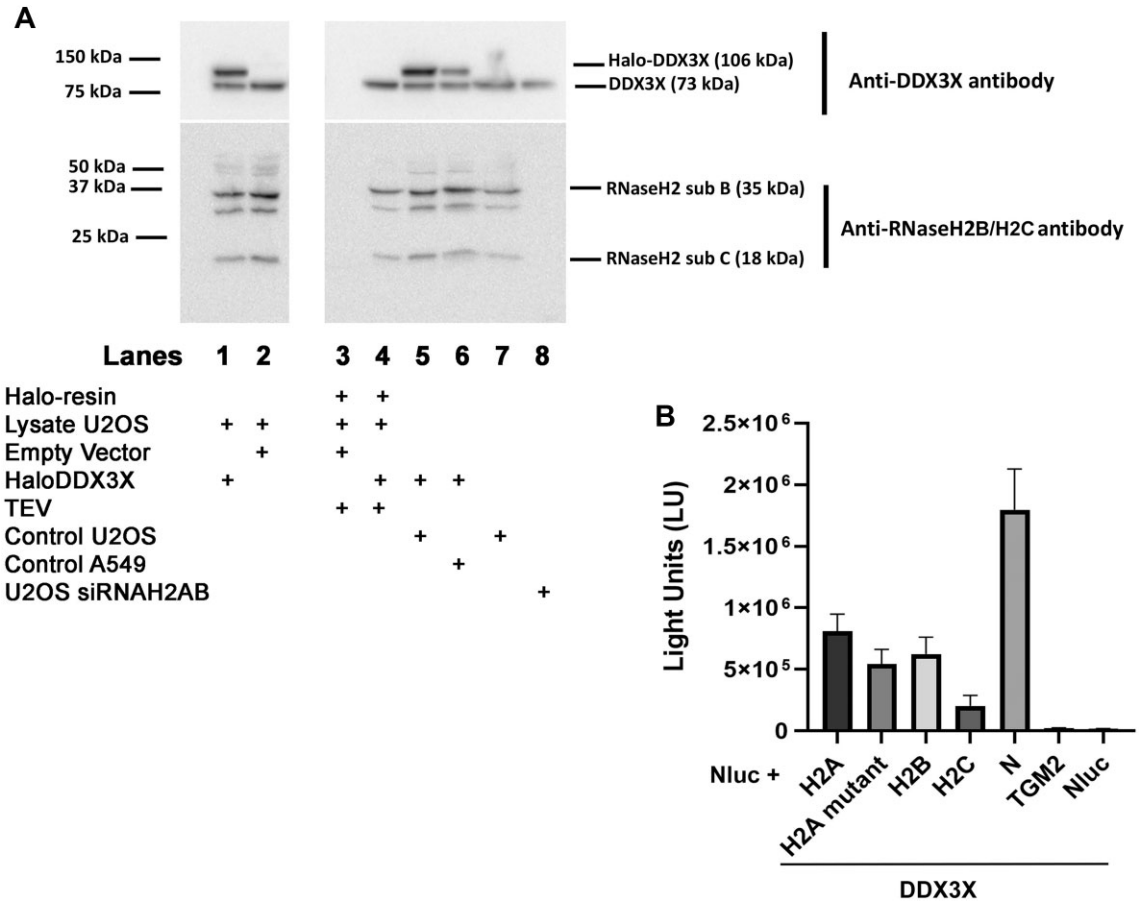


**Figure 6.** DDX3X physically interacts with the RNaseH2 trimeric complex in cell-based assays. (**A**) Cell lysates of U2OS cells transfected with Halo-DDX3X plasmid (lane 1, 10% of the total) or Halo empty vector (lane 2, 10% of the total). After incubation with Halo-link resin and TEV digestion, fractions were analyzed in Western blot with antibodies specific for DDX3X or RNaseH2 B and C subunits. Lane 3, pull-down after TEV digestion in control lysate transfected with empty vector; Lane 4, pull-down after TEV digestion in lysate transfected with Halo-DDX3X; Lanes 5 and 6, control lysates of U2OS and A549 cells transfected with Halo-DDX3X, respectively; Lane 7, control lysate of untreated U2OS cells; Lane 8, control lysate of U2OS cells silenced with siRNA RNaseH2A and B. (**B**) Luminescent pull-down assay. Light units obtained are the means ± SEM of three independent experiments. Nluc-N is the positive control, while Nluc-TGM2 and Nluc alone are the negative controls.

## DDX3X does not stimulate RNaseH1 activity on R-loops

RNaseH1 is involved in R-loop processing, but not in the removal of single rNMPs embedded in dsDNA. Indeed, when tested on the dsDNA substrate containing a single embedded rNMP, RNaseH1 did not show any activity even at high concentrations (Figure 8A, lanes 4–7), while it was able to digest the RNA strand on the synthetic R-loop Substrate **1**, but with a different pattern with respect to RNaseH2 (Figure 8A, compare lanes 9, 10 with lanes 11–14). However, combination of limiting amount of RNaseH1 with increasing concentrations of DDX3X (Figure 8B lanes 9–14) did not result in any synergistic effect with respect to either RNaseH1 (Figure 8B, lane 2) or DDX3X (Figure 8B, lanes 3–8) alone.

Finally, to conclusively show that the synergic effect of the RNaseH2-DDX3X combination was specifically due to the stimulation of RNaseH2 catalytic activity, a RNaseH2 catalytically dead ($RNaseH2_{(KD)}$) mutant was used. Such mutant bears two substitutions D141N-D169N in essential aminoacids of the catalytic site. As expected, when titrated on the synthetic R-loop Substrate **1**, the $RNaseH2_{(KD)}$ mutant did not show any activity, contrary to RNaseH2 wild type (Figure 8C, compare lanes 2–5 with lanes 6–11). When the $RNaseH2_{(KD)}$ mutant was combined with DDX3X, a strong inhibition of DDX3X nuclease activity was observed (Figure 8C, compare lanes 13–15 with lane 12), consistently with the suppressive role of the H2B and C subunits shown in Figure 7A-C. On the contrary, when DDX3X was combined with RNaseH2 wild type, a strong synergic effect was observed as expected (Figure 8C, compare lanes 2, 4 with lanes 16, 17).

Collectively, these results indicated that the observed synergy was specific for the DDX3X-RNaseH2 combination and was absolutely dependent on the RNaseH2 catalytic activity.

## Silencing of DDX3X in human cells causes accumulation of genomic R-loops and phosphorylated RPA foci

In order to determine the effects of the presence or absence of DDX3X/RNaseH2 on the metabolism of endogenous R-loops, immunofluorescence assays with the S9.6 antibody were performed in order to monitor the variations of the signal associated with RNA-DNA hybrids in U2OS cells. Specifically, nuclei were masked by DAPI staining and the mean intensity of S9.6 signal in the nucleus was calculated. As shown in Figure 9A and B, silencing of RNaseH2 alone did not result

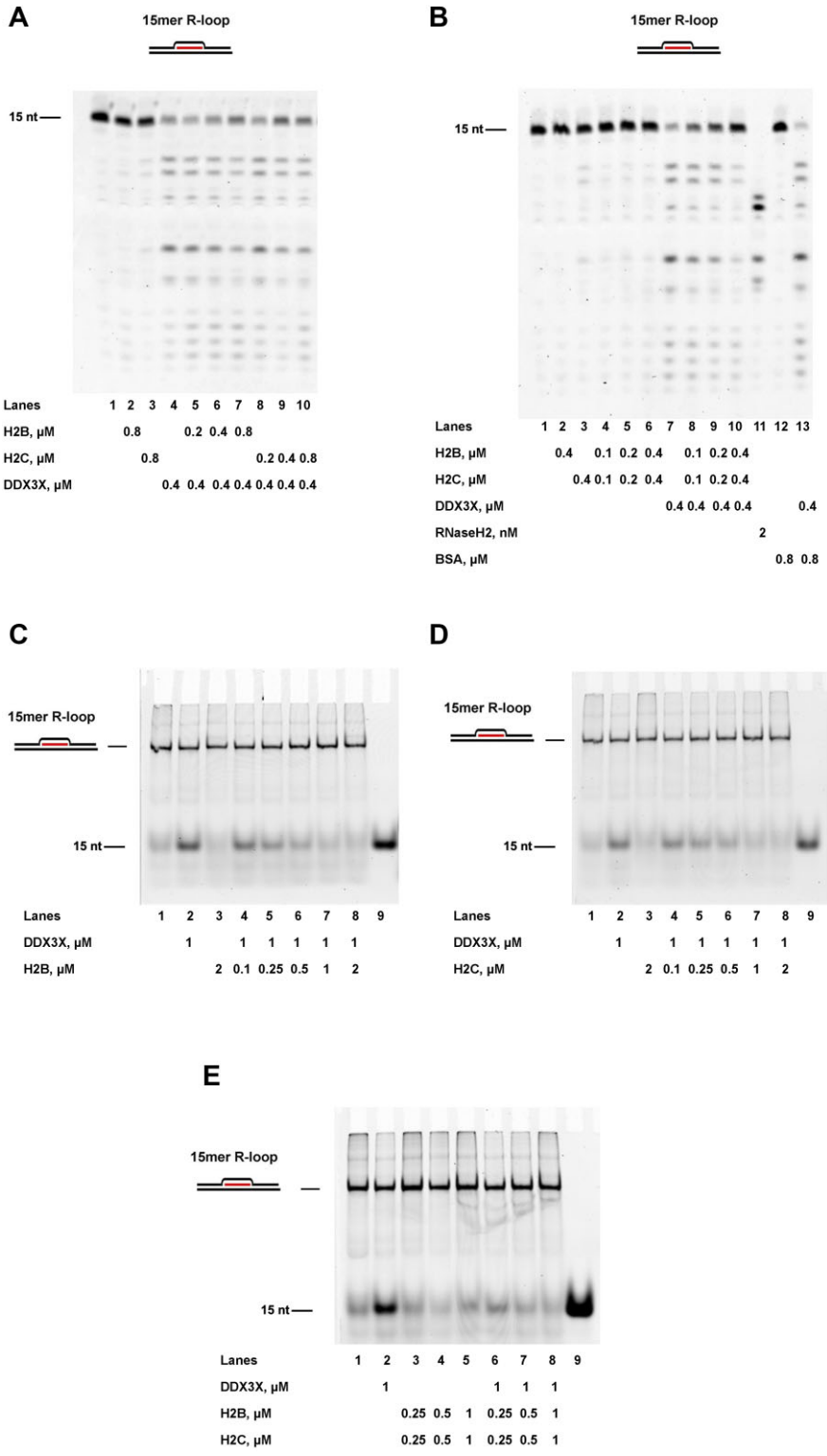


**Figure 7.** The B and C subunits of RNaseH2 inhibit DDX3X activities on R-loops. (**A**) A fixed concentration of human recombinant DDX3X was incubated with substrate 1 either alone (lane 4) or in the presence of increasing concentrations of human recombinant RNaseH2B (lanes 5–7) or H2C (lanes 8–10) subunits. Lane 1, control reaction in the absence of proteins; Lane 2, control reaction in the presence of RNaseH2B; Lane 3, as in lane 2 but in the presence of RNaseH2C. (**B**) Increasing concentrations of a mixture of RNaseH2B and H2C subunits at equimolar ratios were incubated with substrate 1 either alone (lanes 4–6) or in the presence of a fixed amount of DDX3X (lanes 8–10). Lane 1, control reaction in the absence of proteins; Lane 2, control reaction in the presence of RNaseH2B, Lane 3, as in lane 2 but in the presence of RNaseH2C; Lane 7, reaction with DDX3X alone; Lane 11, control reaction with trimeric RNaseH2; Lanes 12, 13, control reactions with BSA alone or in combination with DDX3X. (**C**) Helicase activity of DDX3X alone (lane 2) or in combination with increasing amounts of RNaseH2B subunit (lanes 4–8) on substrate 1. Lane 1, control reaction in the absence of proteins, Lane 3, control reaction in the presence of RNaseH2B alone; Lane 9, 15-mer ssRNA oligonucleotide loaded as marker for the displaced products. (**D**) As in panel C but in the presence of the RNaseH2C subunit. (E). DDX3X alone (lane 2), or increasing concentrations of a mixture of RNaseH2B and H2C subunits at equimolar ratios (lanes 3–5), or a combination of both (lanes 6–8) were incubated on substrate 1 in a helicase assay. Lane 1, control reaction in the absence of proteins; Lane 9, 15-mer ssRNA oligonucleotide loaded as marker for the displaced products.

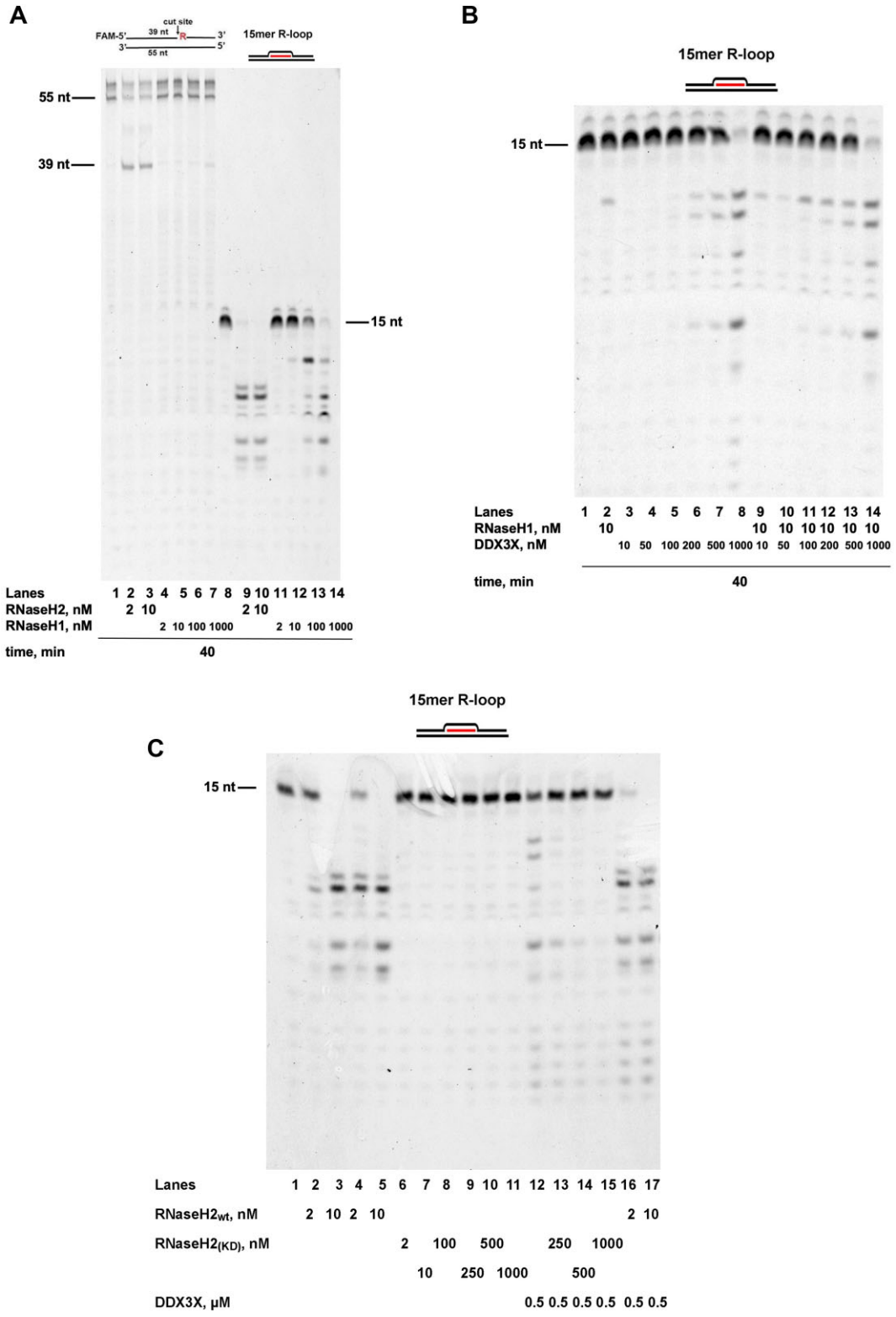


**Figure 8.** DDX3X stimulation is specific for RNaseH2 catalytic activity. (**A**) Increasing concentrations of RNaseH1 were titrated in the presence of substrate 3 (lanes 4–8) or substrate 1 (lanes 11–14). Lanes 1, 8: control reactions in the absence of enzymes; Lanes 2, 3, 9, 10: control reactions with two concentrations of RNaseH2. (**B**) Increasing concentrations of DDX3X were titrated on substrate 1 in the absence (lanes 3–8) or in the presence (lanes 9–14) of a fixed amount of RNaseH1. Lane 1, control reaction in the absence of enzymes; Lane 2, control reaction with RNAseH1 alone. (**C**) Increasing amounts of $RNaseH2_{(KD)}$ catalytically dead mutant were titrated on substrate 1 in the absence (lanes 6–11) or in the presence (Lanes 12–15) of fixed amounts of DDX3X. Lane 1, control reaction in the absence of enzymes; Lanes 2–5, control reaction with RNaseH2wt alone; Lanes 16–17, control reaction with RNaseH2 in the presence of DDX3X.

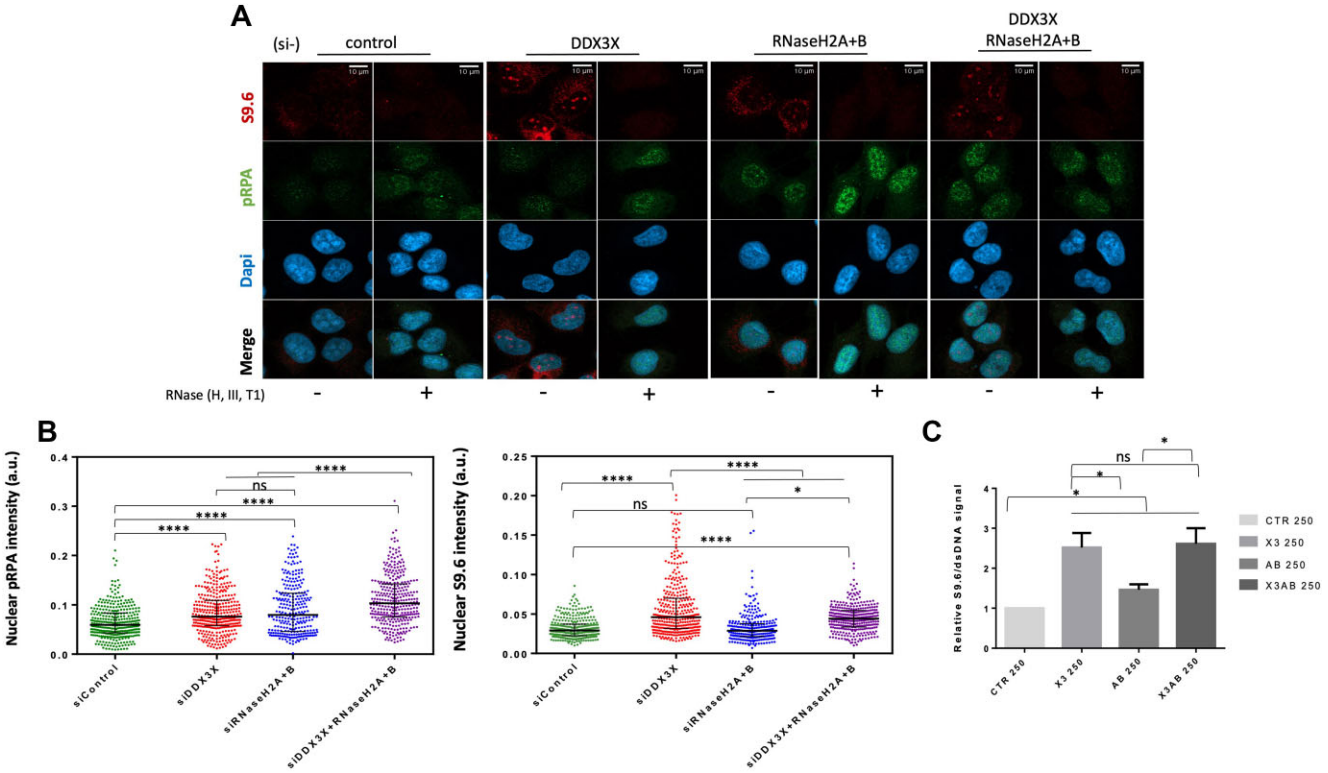


**Figure 9.** Silencing of DDX3X in human cells causes accumulation of genomic R-loops and phosphorylated RPA foci. (**A**) Representative immunofluorescence images obtained using antibodies against RNA:DNA hybrids (S9.6, red) and pRPA (green) after transfection of U2OS cells with control (si-control), DDX3X (siDDX3X), RNaseH2 (siRNaseH2A + siRNAseH2B) or DDX3X and RNaseH2 (siDDX3X + siRNaseH2A + siRNaseH2B) siRNAs. Treatment with RNaseH + RNaseIII + RNaseT1 was used to exclude unspecific S9.6 signals. Scale bars, 10 μm. (**B**) Quantification of mean nuclear intensity of phospho-RPA and S9.6 foci of control and DDX3X, RNaseH2A + B and DDX3x + RNaseH2A + B-depleted U2OS cells. Median with interquartile range (black lines) are indicated. P values were calculated using two-tailed unpaired Student's t test. $*P < 0.05$; $**P < 0.01$; $***P < 0.001$; $****P < 0.0001$; ns, not significant ($P < 0.05$). At least 300 nuclei from three different experiments were analyzed. (**C**) Quantification of RNA:DNA hybrid Dot-blot of genomic DNA ± RNase H for all the siRNA conditions. S9.6 signals are normalized to dsDNA signal. P values were calculated using two-tailed unpaired Student's t test (means ± SEM; $n \geq 2$).

in a significant increase of S9.6 staining with respect to the control cells, while silencing of both RNaseH2 and DDX3X resulted in a higher accumulation of RNA-DNA hybrids with respect to either control cells and RNaseH2 single silencing. Remarkably, silencing of DDX3X alone caused a dramatic increase in RNA-DNA hybrids as revealed by the staining with the S9.6 Ab.

As an independent control, we performed Dot-blot quantification of the RNA-DNA hybrids under single and double silencing conditions. The results were consistent with those of the IF experiments (Figure 9C), in fact we observed an increase of S9.6/dsDNA signals ratio in cells silenced for DDX3X with respect to controls and similar to the signal of double silencing conditions. Also the silencing of RNaseH2 showed a significant increase of the S9.6/dsDNA signal compared with control, but lower than the one observed with silencing of DDX3X alone or in double silencing.

Replication protein A (RPA) is a key upstream checkpoint factor. It has been shown that phosphorylated RPA (pRPA) foci are triggered by R-loops accumulation particularly at stalled replication forks (33–35). Thus, we have used pRPA as a marker of genomic stress induced by R-loops accumulation. As shown in the Figure 9A and B, silencing of either DDX3X or RNaseH2 alone caused an increase in pRPA foci with respect to control cells, which further increased in the double silencing.

## Discussion

RNaseH1 and RNaseH2 are the main enzymes responsible for the processing of RNA-DNA hybrids (12–14,17,18). Since the discovery of the unique ability of RNaseH2 in removing single rNMPs embedded in dsDNA, it has been proposed that RNaseH2 was acting primarily in the RER pathway, while RNaseH1 was believed to deal mostly with R-loops arising from transcription or DNA damage, particularly at the level of DSBs. However, subsequent investigations have revealed an important role of RNaseH2 also in the resolution of R-loops. Development of mutants of yeast RNaseH2, able to cleave RNA-DNA hybrids but no longer proficient in RER, suggested that a subset of R-loops in the yeast genome were specifically processed by RNaseH2. Indeed, it has been shown that the majority of genomic defects in yeast due to the absence if RNaseH2 activity were caused by R-loops accumulation rather than RER defects (36). Subsequent work in yeast investigated in more detail the division of labor between RNaseH1 and H2, showing that RNaseH2 is the major enzyme acting on genomic R-loops in G2/M phases, while RNaseH1 is active during the entire cell cycle, but is recruited to chromatin only in response to specific stress signals induced by R-loops accumulation (18). RNaseH2 has been shown to accumulate at telomeres or DNA damage sites, where it is involved in processing of RNA-DNA hybrids (37,38). However, recent work showed that RNaseH2 is also associated with RNA

polymerase II in a transcription-dependent manner, in proximity of transcription start and termination sites of a subset of genes in human cells. Inactivation of RNaseH2 repressed transcription of those genes and caused accumulation of R-loops (17). Those findings were consistent with the observation that overexpression of RNaseH2 in prostate cancer represses R-loops formation. Inhibition of RNaseH2A expression in such cancer cells caused an increase of R-loops at the TP53 and Androgen Receptor promoters, inducing the accumulation of the repressive epigenetic modifications H3K9me2 and H3K9me3 and reducing gene expression (39). Overall, these results clearly indicate an essential role of RNaseH2 in regulating gene expression and chromatin modifications by processing co-transcriptional R-loops.

In summary, RNaseH2 appears to act at different levels in maintaining genome stability: it is involved in DNA damage response by processing single rNMPs in the RER pathway and processing R-loops at DSBs or stalled replication forks; it regulates gene expression by ensuring a correct balance of R-loops generation during transcription. Several lines of evidence point to a role of the RNA helicase DDX3X, which was the subject of the present study, in the same pathways (22).

DDX3X is involved in nearly all RNA transactions and plays a role in many pathological conditions such as virus infection, inflammation, intellectual disability and cancer (19,40). It participates in gene expression regulation by interacting with transcription factors such as SP1, YY1 and TP53 (41–43) and facilitating the expression of the target genes. Moreover, it can directly enhance the expression of the E-cadherin and IFN-β promoters (44,45). DDX3X is a nucleocytoplasmatic shuttling protein, with a prevalence in the cytoplasm at the steady-state under normal conditions (46). However, it localizes at centrosomes throughout the cell cycle and associates with TP53 at centrosomes during mitosis, playing an import role in regulating chromosome segregation (42). Notably, centrosomes are regions enriched in R-loops and RNaseH2 has been also shown to regulate the accumulation of R-loops at centromeres. DDX3X has also been found to rapidly colocalize at sites of DNA damage in the nucleus of human cells after microirradiation, in a PARP1-dependent fashion, indicating its role in response to DSBs (47). Interestingly, RNaseH2 has been shown to be recruited at DSBs by BRCA2 where it processes DNA damage -induced R-loops (38). Finally, we have previously shown that DDX3X possesses RNaseH2-like activity, being able to recognize and cut single rNMPs embedded in dsDNA and to substitute for RNaseH2 in *in vitro* reconstituted RER reactions (23).

The data presented here indicated that DDX3X has also the ability of processing R-loops in different ways: as a helicase, by displacing the RNA strand, or as a ribonuclease in a similar fashion to RNaseH2, degrading the RNA strand base paired to the DNA. Given the ability of DDX3X to digest ssRNA, coupling helicase and exoribonuclease activities might even lead to the concomitant displacement and degradation of the ssRNA strand of R-loops by DDX3X, which, to the best of our knowledge, might be a property unique to DDX3X among RNA helicases. It is possible that the local chromatin context and/or additional auxiliary factors might regulate the balance between these alternative modes. The role of DDX3X in R-loops processing was found to be physiologically relevant, since silencing of DDX3 in human cells caused an accumulation of genomic R-loops.

However, an additional result shown here was that DDX3X physically interacted and stimulated several-fold the catalytic activity of RNaseH2 both on R-loops and single rNMPs. Interaction of DDX3X with the RNaseH2B and H2C subunits either separately or in complex with a catalytically dead RNaseH2A mutant, repressed both the helicase and the nuclease activities of DDX3X, thus conclusively demonstrating that the increased digestion efficiency observed was exclusively due to the catalytic activity of RNaseH2.

It has been already suggested that the heterodimer formed by the H2B and H2C subunit can be stably formed in cells acting as a platform to recruit additional proteins. For example, the H2B subunit harbors a PCNA-interacting domain and was found to physically interact with PCNA. Such interaction did not influence the catalytic activity of the human RNaseH2 complex, at least *in vitro*, but was found to help specific recruitment of human RNaseH2 to DNA replication and repair sites (48). The findings presented here suggest that DDX3X can also act as a scaffold for RNaseH2, by directly interacting with all three subunits and increasing its catalytic activity. Given the plethora of known protein-protein interactors of DDX3X, its binding to RNaseH2 can also regulate the subcellular localization of RNaseH2 at specific genomic sites, for example the TP53 promoter, the centromeres or the DSBs, where DDX3X and RNaseH2 proteins have been shown to localize in different studies. In addition, it has been shown that deregulated R-loop processing in the nucleus leads to the accumulation of cytoplasmic R-loops, which are potent activators of the innate immunity response through the cGAS and TLR3 receptors (49,50). DDX3X in the cytoplasm plays a role in innate immunity, acting downstream of the TLR3-TRIF-TRAF3 signaling pathway by activating the TBK1-IKKα/β axis (51). The results presented here showing that DDX3X alone can process R-loops, may also implicate its role in processing aberrant cytoplasmic R-loops, generated in the presence dysfunctional RNaseH2 or Senataxin.

The results of our silencing experiments clearly showed that suppressing DDX3X alone in a RNaseH1 and H2 proficient background resulted in higher levels of RNA-DNA hybrids, with respect to those observed in cells silenced for RNaseH2 alone. This may suggest a role of DDX3X in limiting R-loops accumulation which is independent from RNaseH2. On the other hand, the increase of pRPA foci was similar in either DDX3X or RNaseH2 silenced cells and further increased upon double silencing. Since pRPA marks only a subset of R-loops, mainly those linked to stalled replication forks, it is possible that at the level of replication forks DDX3X indeed primarily works as a cofactor of RNaseH2, increasing its efficiency, while it has a more general role in preventing aberrant R-loop accumulation throughout the genome, for example at the level of highly transcribed genes, consistently with its roles as a transcriptional regulator. This aspect warrants further investigation.

Thus, based on the present and previous results, it is possible to envisage the presence of alternative mechanisms for RNA-DNA hybrid tolerance involving DDX3X and RNaseH2, either acting alone or in combination. The next step will be to understand the spatial and temporal regulation of these different pathways as a function of cell cycle stage and cellular stress and their relevance in pathological conditions such as AGS and cancer.

## Data availability

All the relevant data underlying this article are available in the article and in its online supplementary material. Raw datasets (gel quantifications) will be shared on reasonable request to the corresponding author.

## Supplementary data

Supplementary Data are available at NAR Online.

## Funding

Italian Association for Cancer Research AIRC Investigator Grant [IG2022-27833 to G.M.]; Italian Association for Cancer Research AIRC [IG2020 no. 24448 to E.C.]. Funding for open access charge: Italian Association for Cancer Research.

## Conflict of interest statement

None declared.

## References

1. Petereman,E., Lam,L. and Zou,L. (2022) Sources, resolution and physiological relevance of R-loops and RNA-DNA hybrids. *Nat. Rev. Mol. Cell Biol.*, **23**, 521–540.
2. Brickner,J., Garzon,J.L. and Cimprich,K.A. (2022) Walking a tightrope: the complex balancing act of R-loops in genome stability. *Mol. Cell*, **82**, 2267–2297.
3. Lee,D.Y. and Clayton,D.A. (1998) Initiation of mitochondrial DNA replication by transcription and R-loop processing. *J. Biol. Chem.*, **273**, 30614–30621.
4. Crossley,M.P., Bocek,M. and Cimprich,K.A. (2019) R-loops as cellular regulators and genomic threats. *Mol. Cell.*, **73**, 398–411.
5. Castillo-Guzman,D. and Chédin,F. (2021) Defining R-loop classes and their contributions to genome instability. *DNA Repair (Amst.)*, **106**, 103182.
6. Liu,Q., Liu,Y., Shi,Q., Su,H., Wang,C., Birchler,J.A. and Han,F. (2021) Emerging roles of centromeric RNAs in centromere formation and function. *Genes Genomics*, **43**, 217–226.
7. Sanz,L.A., Hartono,S.R., Lim,Y.W., Steyaert,S., Rajpurkar,A., Ginno,P.A., Xu,X. and Chédin,F. (2016) Prevalent, dynamic, and conserved R-loop structures associate with specific epigenomic signatures in mammals. *Mol. Cell*, **63**, 167–178.
8. Skourti-Stathaki,K., Proudfoot,N.J. and Gromak,N. (2011) Human senataxin resolves RNA-DNA hybrids formed at transcriptional pause sites to promote Xrn2-dependent termination. *Mol. Cell*, **42**, 794–805.
9. Kim,S., Kang,N., Park,S.H., Wells,J., Hwang,T., Ryu,E., Kim,B.G., Hwang,S., Kim,S.J., Kang,S., *et al.* (2020) ATAD5 restricts R-loop formation through PCNA unloading and RNA helicase maintenance at the replication fork. *Nucleic Acids Res.*, **48**, 7218–7238.
10. Niehrs,C. and Luke,B. (2020) Regulatory R-loops as facilitators of gene expression and genome stability. *Nat. Rev. Mol. Cell Biol.*, **21**, 167–178.
11. Marnef,A. and Legube,G. (2021) R-loops as Janus-faced modulators of DNA repair. *Nat. Cell Biol.*, **23**, 305–313.
12. Parajuli,S., Teasley,D.C., Murali,B., Jackson,J., Vindigni,A. and Stewart,S.A. (2017) Human ribonuclease H1 resolves R-loops and thereby enables progression of the DNA replication fork. *J. Biol. Chem.*, **292**, 15216–15224.
13. El Hage,A., French,S.L., Beyer,A.L. and Toller,D. (2010) Loss of Topoisomerase I leads to R-loop-mediated transcriptional blocks during ribosomal RNA synthesis. *Genes Dev.*, **24**, 1546–1558.
14. Lima,W.F., Murray,H.M., Damle,S.S., Hart,C.E., Hung,G., De Hoyos,C.L., Liang,X.-H. and Crooke,S.T. (2016) Viable RNaseH1 knockout mice show RNaseH1 is essential for R loop processing, mitochondrial and liver function. *Nucleic Acids Res.*, **44**, 5299–52312.
15. Reijns,M.A. and Jackson,A.P. (2014) Ribonuclease H2 in health and disease. *Biochem. Soc. Trans.*, **42**, 717–725.
16. Sparks,J.L., Chon,H., Cerritelli,S.M., Kunkel,T.A., Johansson,E., Crouch,R.J. and Burgers,P.M. (2012) RNase H2-initiated ribonucleotide excision repair. *Mol. Cell*, **47**, 980–986.
17. Cristini,A., Tellier,M., Constantinescu,F., Accalai,C., Albulesci,L.O., Heiringhoff,R., Bery,N., Sordet,O., Murphy,S. and Gromak,N. (2022) RNase H2, mutated in Aicardi-Goutières syndrome, resolves co-transcriptional R-loops to prevent DNA breaks and inflammation. *Nat. Commun.*, **26**, 2961.
18. Lockhart,A., Pires,V.B., Bento,F., Kellner,V., Luke-Glaser,L., Yakoub,G., Ulrich,H.D. and Luke,B. (2019) RNase H1 and H2 Are differentially regulated to process RNA-DNA hybrids. *Cell. Rep.*, **29**, 2890–2900.
19. Mo,J., Liang,H., Su,C., Li,P., Chen,J. and Zhang,B. (2021) DDX3X: structure, physiologic functions and cancer. *Mol. Cancer.*, **20**, 38.
20. Cargill,M., Venkataraman,R. and Lee,S. (2021) DEAD-Box RNA helicases and genome stability. *Genes (Basel)*, **12**, 1471.
21. Riva,V. and Maga,G. (2019) From the magic bullet to the magic target: exploiting the diverse roles of DDX3X in viral infections and tumorigenesis. *Future Med. Chem.*, **11**, 1357–1381.
22. Secchi,M., Lodola,C., Garbelli,A., Bione,S. and Maga,G. (2022) DEAD-Box RNA helicases DDX3X and DDX5 as oncogenes or oncosuppressors: a network perspective. *Cancers (Basel)*, **14**, 3820.
23. Riva,V., Garbelli,A., Casiraghi,F., Arena,F., Trivisani,C.I., Gagliardi,A., Bini,L., Schroeder,M., Maffia,A., Sabbioneda,S., *et al.* (2020) Novel alternative ribonucleotide excision repair pathways in human cells by DDX3X and specialized DNA polymerases. *Nucleic Acids Res.*, **48**, 11551–11565.
24. de Bisschop,G., Ameur,M., Ulryck,N., Benattia,F., Ponchon,L., Sargueil,B. and Chamond,N. (2019) HIV-1 gRNA, a biological substrate, uncovers the potency of DDX3X biochemical activity. *Biochimie*, **164**, 83–94.
25. Floor,S.N., Condon,K.J., Sharma,D., Jankowsky,E. and Doudna,J.A. (2016) Autoinhibitory interdomain interactions and subfamily specific extensions redefine the catalytic core of the human DEAD-box protein DDX3. *J. Biol. Chem.*, **291**, 2412–2421.
26. Chon,H., Vassilev,C.A., DePamphilis,M.L., Zhao,Y., Zhang,J., Burgers,P.M., Crouch,R.J. and Cerritelli,S.M. (2009) Contributions of the two accessory subunits, RNASEH2B and RNASEH2C, to the activity and properties of the human RNase H2 complex. *Nucleic Acids Res.*, **37**, 96–110.
27. Secchi,M., Bazzigaluppi,E., Brigatti,C., Marzinotto,I., Tresoldi,C., Rovere-Querini,P., Poli,A., Castagna,A., Scarlatti,G., Zangrillo,A., *et al.* (2020) COVID-19 survival associates with the immunoglobulin response to the SARS-CoV-2 spike receptor binding domain. *J. Clin. Invest.*, **130**, 6366–6378.
28. Dowling,J.W., Smith,J.R. and Forero,A. (2024) Protocol for detection of in vitro R-loop formation using dot blots. *STAR Protoc*, **5**, 102857.
29. Smolka,J.A., Sanz,L.A., Hartono,S.R. and Chédin,F. (2021) Recognition of RNA by the S9.6 antibody creates pervasive artifacts when imaging RNA:DNA hybrids. *J. Cell. Biol.*, **220**, e202004079.
30. Mentegari,E., Crespan,E., Bavagnoli,L., Kissova,M., Bertoletti,F., Sabbioneda,S., Imhof,R., Sturla,S.J., Nilforoushan,A., Hübscher,U., *et al.* (2017) Ribonucleotide incorporation by human DNA polymerase η impacts translesion synthesis and RNase H2 activity. *Nucleic Acids Res.*, **45**, 2600–2614.
31. Garbelli,A., Beermann,S., Di Cicco,G., Dietrich,U. and Maga,G. (2011) A motif unique to the human DEAD-box protein DDX3 is important for nucleic acid binding, ATP hydrolysis, RNA-DNA unwinding and HIV-1 replication. *PLoS One*, **6**, e19810.

32. Lodola,C., Secchi,M., Sinigiani,V., De Palma,A., Rossi,R., Perico,D., Mauri,P.L. and Maga,G. (2023) Interaction of SARS-CoV-2 nucleocapsid protein and human RNA helicases DDX1 and DDX3X modulates their activities on double-stranded RNA. *Int. J. Mol. Sci.*, **24**, 5784.
33. Nguyen,H.D., Yadav,T., Giri,S., Saez,B., Graubert,T.A. and Zou,L. (2017) Functions of replication protein A as a sensor of R loops and a regulator of RNaseH1. *Mol. Cell.*, **65**, 832–847.
34. Promonet,A., Padioleau,I., Liu,Y., Sanz,L., Biernacka,A., Schmitz,A.L., Skrzypczak,M., Sarrazin,A., Mettling,C., Rowicka,M., *et al.* (2020) Topoisomerase 1 prevents replication stress at R-loop-enriched transcription termination sites. *Nat. Commun.*, **11**, 3940.
35. Ashley,A.K., Shrivastav,M., Nie,J., Amerin,C., Troksa,K., Glanzer,J.G., Liu,S., Opiyo,S.O., Dimitrova,D.D., Le,P., *et al.* (2014) DNA-PK phosphorylation of RPA32 Ser4/Ser8 regulates replication stress checkpoint activation, fork restart, homologous recombination and mitotic catastrophe. *DNA Repair (Amst.)*, **21**, 131–139.
36. Chon,H., Sparks,J.L., Rychlik,M., Nowotny,M., Burgers,P.M., Crouch,R.J. and Cerritelli,S.M. (2013) RNase H2 roles in genome integrity revealed by unlinking its activities. *Nucleic Acids Res.*, **41**, 3130–3143.
37. Graf,M., Bonetti,D., Lockhart,A., Serhal,K., Kellner,V., Maicher,A., Jolivet,P., Teixeira,M.T. and Luke,B. (2017) Telomere length determines TERRA and R-loop regulation through the cell cycle. *Cell*, **170**, 72–85.
38. D'Alessandro,G., Whelan,D.R., Howard,S.M., Vitelli,V., Renaudin,X., Adamowicz,M., Iannelli,F., Jones-Weiner,C.W., Lee,M., Matti,V., *et al.* (2018) BRCA2 controls DNA:RNA hybrid level at DSBs by mediating RNase H2 recruitment. *Nat. Commun.*, **9**, 5376.
39. Kimura,N., Takayama,K.I., Yamada,Y., Kume,H., Fujimura,T. and Inoue,S. (2022) Ribonuclease H2 subunit A preserves genomic integrity and promotes prostate cancer progression. *Cancer Res. Commun.*, **2**, 870–883.
40. Schröder,M. (2010) Human DEAD-box protein 3 has multiple functions in gene regulation and cell cycle control and is a prime target for viral manipulation. *Biochem. Pharmacol.*,; **79**, 297–306.
41. Chao,C.H., Chen,C.M., Cheng,P.L., Shih,J.W., Tsou,A.P. and Lee,Y.H. (2006) DDX3, a DEAD box RNA helicase with tumor growth-suppressive property and transcriptional regulation activity of the p21waf1/cip1 promoter, is a candidate tumor suppressor. *Cancer Res.*, **66**, 6579–6588.
42. Chen,W.J., Wang,W.T., Tsai,T.Y., Li,H.K. and Lee,Y.W. (2017) DDX3 localizes to the centrosome and prevents multipolar mitosis by epigenetically and translationally modulating p53 expression. *Sci. Rep.*, **7**, 9411.
43. Yang,F., Fang,E., Mei,H., Chen,Y., Li,H., Li,D., Song,H., Wang,J., Hong,M., Xiao,W., *et al.* (2019) Cis-Acting circ-CTNNB1 promotes β-catenin signaling and cancer progression via DDX3-mediated transactivation of YY1. *Cancer Res.*, **79**, 557–571.
44. Botlagunta,M., Vesuna,F., Mironchik,Y., Raman,A., Lisok,A., Winnard,P Jr, Mukadam,S., Van Diest,P., Chen,J.H., Farabaugh,P., *et al.* (2008) Oncogenic role of DDX3 in breast cancer biogenesis. *Oncogene*, **27**, 3912–3922.
45. Atkinson,S.C., Heaton,S.M., Audsley,M.D., Kleifeld,O. and Borg,N.A. (2021) TRIM25 and DEAD-Box RNA helicase DDX3X cooperate to regulate RIG-I-mediated antiviral immunity. *Int. J. Mol. Sci.*, **22**, 9094.
46. Brennan,R., Haap-Hoff,A., Gu,L., Gautier,V., Long,A. and Schröder,M. (2018) Investigating nucleo-cytoplasmic shuttling of the human DEAD-box helicase DDX3. *Eur. J. Cell Biol.*, **97**, 501–511.
47. Cargill,M.J., Morales,A., Ravishankar,S. and Warren,E.H. (2021) RNA helicase, DDX3X, is actively recruited to sites of DNA damage in live cells. *DNA Repair (Amst.)*, **103**, 103137.
48. Bubeck,D., Reijns,M.A., Graham,S.C., Astell,K.R., Jones,E.Y. and Jackson,A.P. (2011) PCNA directs type 2 RNase H activity on DNA replication and repair substrates. *Nucleic Acids Res.*, **39**, 3652–3666.
49. Mackenzie,K.J., Carroll,P., Lettice,L., Tarnauskaitė,Z., Reddy,K., Dix,F., Revuelta,A., Abbondati,E., Rigby,R.E., Rabe,B., *et al.* (2016) Ribonuclease H2 mutations induce a cGAS/STING-dependent innate immune response. *EMBO J.*, **35**, 831–844.
50. Crossley,M.P., Song,C., Bocek,M.J., Choi,J.H., Kousorous,J., Sathirachinda,A., Lin,C., Brickner,J.R., Bai,G., Lans,H., *et al.* (2023) R-loop-derived cytoplasmic RNA-DNA hybrids activate an immune response. *Nature*, **613**, 187–194.
51. Su,C., Tang,Y.D. and Zheng,C.(2021) DExD/H-box helicases: multifunctional regulators in antiviral innate immunity. *Cell. Mol. Life Sci.*, **79**, 2.


**Received:** November 28, 2023. **Revised:** July 18, 2024. **Editorial Decision:** August 7, 2024. **Accepted:** August 12, 2024